GIScience & Remote Sensing

ISSN: 1548-1603 (Print) 1943-7226 (Online) Journal homepage: www.tandfonline.com/journals/tgrs20

Insights into global change effects on a Mediterranean rural landscape with badlands: a remote sensing approach on climate and land cover changes

Annalisa Sannino, Ebrahim Ghaderpour, Giulia Iacobucci, Maurizio Del Monte & Francesca Vergari

To cite this article: Annalisa Sannino, Ebrahim Ghaderpour, Giulia Iacobucci, Maurizio Del Monte & Francesca Vergari (2026) Insights into global change effects on a Mediterranean rural landscape with badlands: a remote sensing approach on climate and land cover changes, GIScience & Remote Sensing, 63:1, 2662163, DOI: 10.1080/15481603.2026.2662163

To link to this article: https://doi.org/10.1080/15481603.2026.2662163

GISCIENCE & REMOTE SENSING
2026, VOL. 63, NO. 1, 2662163
https://doi.org/10.1080/15481603.2026.2662163

Taylor & Francis
by informa

RESEARCH ARTICLE

OPEN ACCESS Check for updates

Insights into global change effects on a Mediterranean rural landscape with badlands: a remote sensing approach on climate and land cover changes

Annalisa Sannino, Ebrahim Ghaderpour, Giulia Iacobucci, Maurizio Del Monte and Francesca Vergari

Earth Sciences Department, Sapienza University of Rome, Rome, Italy

ABSTRACT

Over the past decades, the combined effects of climate, in terms of thermo-pluviometric variability, and land-cover transformations have profoundly reshaped Mediterranean rural landscapes, altering their ecological balance and geomorphological stability. These pressures are particularly critical in badland environments, fragile erosional systems marked by steep slopes, limited vegetation, and dense networks of gullies and mass-wasting features, often associated with rural landscapes. This study investigates four decades (1984–2023) of vegetation dynamics within the Orcia River catchment in Tuscany (Italy), a UNESCO World Heritage Site containing representative sub-humid badlands, with the aim of explaining these dynamics in relation to climate variability and land-use changes. Monthly Normalized Difference Vegetation Index (NDVI) time series derived from Landsat imagery were analyzed together with MODIS Land Surface Temperature (LST), Global Precipitation Measurement (GPM) data, and ground-based meteorological records. Regional Land Use and Land Cover (LULC) maps were analyzed to evaluate land-cover transitions. Long-term vegetation and climate trends were assessed using the Mann–Kendall test and Sen's slope estimator on NDVI pixels filtered using the Pixel Quality Assessment (PQA) band and on climatic satellite and ground-based datasets (2004–2023). Results revealed a steady and statistically significant greening trend across the study area since 1984, with most pixels showing NDVI increases of about 0.005 units per year. Vegetation changes were mostly insignificant or slightly negative during 1984–2003, whereas a more pronounced increase occurred after 2004 (0.005–0.010 units yr^{-1}, up to 0.015 along river corridors). Satellite and ground-based meteorological station data showed a warming trend, particularly in minimum temperatures, whereas precipitation remained generally stable. About 42% of the area underwent land-cover change, primarily due to forest expansion and a reduction in grazing and sparsely vegetated areas, mostly linked to the badlands surface. NDVI–LULC intersection analyses showed that most NDVI variations coincided with land-use transitions, while NDVI increases in stable areas suggest management-driven change in vegetation cover. This greening process seems to be enhanced by the registered warming trend, as suggested by the positive correlation between MODIS-NDVI and MODIS-LST values within the southern forested region. Our findings demonstrate the synergistic influence of climate warming and land-cover change on Mediterranean landscapes. The general greening process, which leads to a reduction of badland surfaces, appears to be driven by more favourable climate conditions, which enhance vegetation vigour, and by the abandonment of traditional agricultural practices, allowing natural vegetation recovery.

ARTICLE HISTORY
Received 21 November 2025
Accepted 9 April 2026

KEYWORDS
NDVI; badlands; landsat; MODIS; GPM

1. Introduction

Most contemporary landscapes are the result of long-term interactions between human societies and their surrounding environments, in which natural systems have been progressively modified, managed, and reorganized to meet human needs. This is particularly true for European and especially Mediterranean landscapes, where centuries of human presence have gradually left a visible imprint on hillslopes, valleys, and plains (Brandolini et al. 2023; Blondel 2006; Brandolini et al. 2020). Traditional agro-silvo-pastoral

CONTACT Annalisa Sannino annalisa.sannino@uniroma1.it
Supplemental data for this article can be accessed online at https://doi.org/10.1080/15481603.2026.2662163.

systems such as chestnut orchards, terraced vineyards and olive groves, mixed cropping systems, and rotational grazing have historically created fine-grained mosaics of fields, pastures, and woodlands closely interlaced with rural settlements (Agnoletti 2007; Gallardo et al. 2023; Kizos, Dalaka, and Petanidou 2010).

Ongoing global change is profoundly reshaping terrestrial ecosystems, with cascading effects on landscape dynamics and on the ecosystem services (Gilman and Wu 2023; Martinez-Harms et al. 2017). Traditional rural landscapes are undergoing noticeable transformations driven by both direct (e.g. socio-economic pressure) and indirect (e.g. climate change) factors. Among socio-economic pressures, the depopulation of inland areas, the abandonment of agricultural land, and the decline of traditional land-use practices like grazing and transhumant sheep-farming are widely recognized as major drivers of landscape change, which often result in land degradation and/or simplification (Bajocco et al. 2012; Gabriele et al. 2023).

Mediterranean rural landscapes are often shaped by the combined effects of contrasting climatic conditions, characterized by intense precipitation concentrated in short periods, strong anthropogenic pressure, and the widespread presence of highly erodible bedrocks. These factors promote the development of highly degraded landscapes known as badlands, often associated with agricultural areas. Badlands are highly dissected erosion landscapes characterized by sparse vegetation and intense rill and gully development, typically occurring on highly erodible substrates (Bryan and Yair 1982; Harvey 2004). These erosion landforms occur not only in arid environments but also where vegetation is limited by long-standing anthropogenic pressures, such as deforestation, rather than by climatic aridity. Badlands enhance rural landscape heterogeneity and contribute substantially to its scenic and cultural value (Amici et al. 2017). Indeed, this distinctive erosion landform is progressively being designated as a geosite worldwide (Zgłobicki et al. 2018), which often entails its inclusion within specific conservation and legal protection frameworks. Badlands represent a valuable natural laboratory for investigating geomorphological processes (Ciccacci et al. 2008; Colacicco et al. 2025; Del Monte 2017; Neugirg et al., 2016; Stark et al. 2020; Vergari et al. 2013), so that their morphodynamics can be used as an indirect indicator of how wider rural landscapes respond to ongoing global change. Indeed, their evolution, in terms of spatial extension and erosion rate, can reflect changes in the land management (Vergari et al. 2025) and in temperature and precipitation regimes (Nadal-Romero et al. 2021). Recent studies have quantified a badland reduction trend, associated with a reduction of hillslope denudation rates, common in the Italian peninsula, but also in other Mediterranean areas (Piccarreta et al., 2006; Aucelli et al., 2014; Torri et al. 2013; Amici et al. 2017; Bosino, Omran, and Maerker 2019; Llena et al. 2019; Coratza and Parenti 2021; Vergari et al. 2025). The main causes have been generally attributed to land use changes, such as agricultural land expansion, a successive agricultural abandonment, often involving the levelling or the natural greening of badlands and, simultaneously, the loss of agrarian biodiversity (Agnoletti, 2012, 2022; Torri et al. 2013; Vergari et al. 2025).

Beyond socio-economic drivers of land use change, climate change plays an increasingly important role in shaping Mediterranean landscapes by altering the ecological conditions that underpin their configuration. It affects vegetation dynamics by modifying temperature and precipitation regimes, which regulate plant productivity, drought stress, and species composition (Vicente-Serrano et al. 20123). Notably, vegetation responses are highly heterogeneous across the bioclimatic zones. For instance, in Mediterranean areas, vegetation responses to climate change are mainly driven by reduced precipitation and increased drought, which suppress plant growth and alter species composition, with negative effects on ecosystem productivity (Feller and Vaseva 2014). In contrast, sub-Mediterranean zones show greater adaptive capacity, with rising species richness and an upslope expansion of thermophilous and shrubby species promoted by warming, although drought can still limit growth and reshape community composition (Chelli et al.,, 2017).

The role of climatic shifts in driving vegetation recovery and badland greening has not been fully explored. Most existing studies on badland areas primarily focus on quantifying changes in erosion rates, either through direct measurements of denudation and sediment yield or through detailed geomorphological mapping. While these approaches provide very detailed information at the site scale, they often suffer from limited spatial representativeness and relatively short observation periods, which hampers the possibility of reconstructing long-term landscape trajectories compared with what can be achieved using multi-decadal satellite imagery, albeit at the cost of reduced spatial resolution of surface features. A growing number of studies have started to exploit satellite imagery to investigate badland areas, typically by focusing on badlands inventory and vegetation development inside the badland surface

(Bosino, Omran, and Maerker 2019; Nadal-Romero, Vicente-Serrano, and Jiménez 2012). However, many applications rely on relatively limited image sets, frequently using a single image per year and selecting scenes on the basis of user-defined criteria such as cloud cover or data quality. This practice can introduce temporal gaps and enhance seasonal and interannual sampling biases in vegetation analyses, ultimately restricting the ability to reconstruct continuous, long-term trajectories of landscape change. Furthermore, these analyses often pay less attention to the broader landscape context in which badlands are embedded and to the concurrent evolution of surrounding land covers.

In this context, monitoring these transformations and investigating their drivers and consequences is therefore crucial (Kumar et al. 2025), particularly at regional scales, where the detection and quantification of change are inherently scale-dependent and patterns observed at coarser resolutions may underestimate or exaggerate local-scale dynamics (Šímová and Gdulová 2012; Wu and Li 2009). Such assessments provide the scientific basis for sustainable spatial planning, risk mitigation, and the protection of fragile rural landscapes, especially in regions where socio-economic pressures and climate change interact in complex ways.

Earth observation data from satellite platforms represent a powerful tool for monitoring environmental dynamics and assessing landscape transformations over time. Multitemporal satellite products, such as Landsat, MODIS Land Surface Temperature (LST), and the Global Precipitation Measurement (GPM) mission, provide valuable datasets for assessing changes in vegetation cover, climatic variables, and surface processes. Spectral vegetation indices derived from multispectral sensors are widely employed to detect variations in chlorophyll content and to infer patterns of biomass change, vegetation stress, and phenological development. The strengths and limitations of different vegetation indices have been extensively discussed in the literature (Xue and Su 2017). Among them, the Normalized Difference Vegetation Index (NDVI) is one of the most commonly applied, owing to its simplicity, robustness, and proven utility across diverse environmental settings (Bajocco et al. 2019; De Angelis, Bajocco, and Ricotta 2012; Huang et al. 2021; Pettorelli et al. 2005). When derived from the Landsat archive, NDVI provides a consistent record of vegetation dynamics dating back to the early 1980s, with a spatial resolution of 30 meters (Cavalli et al. 2022; Manes et al. 2010; Ricotta, Corona, and Marchetti 1999). However, data continuity may be affected by cloud cover, sensor limitations, and atmospheric interference. The advent of Google Earth Engine has further revolutionized the use of these satellite products, providing an efficient cloud-based platform for accessing, processing, and analyzing large volumes of imagery over space and time. In addition, it offers harmonized, analysis-ready datasets and built-in tools for atmospheric correction, cloud masking, and temporal compositing, thereby facilitating consistent multi-sensor and multi-temporal assessments of landscape change (Shelestov et al. 2017; Velastegui-Montoya and Montalván-Burbano, 2023).

Building upon this background, this study investigates long-term vegetation dynamics at a fine regional scale in a representative Italian rural landscape characterized by badlands, with the overarching hypothesis that climate variability and land-use transitions jointly drive vegetation change and, indirectly, the evolution of badland areas.

Specifically, the study aims to answer the following research questions:

1. Is the study area undergoing a revegetation process that may contribute to landscape transformation and the gradual reduction of badlands landforms?
2. Are there detectable seasonal long-term trends in precipitation and temperature?
3. Is there a correlation between climatic variables and vegetation dynamics?
4. What is the role of land-use transformations in driving landscape change?

Specifically, we perform a long-term (1984–2023) regional assessment of Landsat-based NDVI time series derived in Google Earth Engine, in which scenes are quality-filtered and composited at a monthly resolution to maximize data availability. Climate information includes satellite-derived products and ground-based records from local meteorological stations, enabling a comparison of long-term climatic trends derived from the different data sources. For the last two decades (2000–2023), multi-temporal trend analyses were performed on climate variables, and MODIS-derived NDVI was implemented to assess the correlation between vegetation dynamics and climatic factors. Land-use trajectories are reconstructed from a set of high-resolution regional maps, which provide finer spatial detail (1:10,000 and 1:25,000) and a more informative temporal sampling than standard products such as CORINE Land Cover or MODIS Land Cover, typically characterized by coarser resolution or less frequent updates. This multi-source framework enables the reconstruction of consistent, multi-decadal trajectories of landscape change, in which badland areas are therefore not analyzed as isolated landforms, but as integral components of the rural landscape and as sensitive proxies of how global-change drivers propagate through the broader socio-ecological system.

2. Materials and methods

2.1. Study region

The study area encompasses the drainage basin of the Orcia River, a 70 km-long tributary of the Ombrone River, situated in the southern Tuscany region, Italy (Figure 1). The Orcia River originates from the southwestern slopes of Monte Cetona and flows into the Ombrone River, the second most important river in Tuscany after the Arno. The basin covers approximately 885.28 km^2 and includes the renowned Val d'Orcia, a UNESCO World Heritage Site recognized for its exceptional natural and cultural landscapes (UNESCO). Approximately 69% of the basin lies within the boundaries of the UNESCO World Heritage Site, encompassing the entire Upper and Middle Orcia Valley. The area was designated as a World Heritage Site in 2004 as an outstanding example of a Renaissance landscape, reflecting ideals of good governance, agrarian planning, and aesthetic harmony. Celebrated by painters of the Sienese School, the Val d'Orcia has long served as a symbolic representation of the Renaissance vision of the landscape as the product of a balanced interaction between humans and nature.

Furthermore, owing to its location in the Mediterranean region, widely recognized as a climate change hotspot (Tuel and Eltahir 2020), it represents a key study site for exploring climate-related processes and impacts.

Currently, the landscape is mainly characterized by gently rolling hills, extensive agricultural fields, patches of woodland, and reduced badland formations, resulting in the visual impression of a long-lasting, natural environment. The region is internationally renowned for its wine and olive oil production, for being the home to historic hilltop towns such as Montalcino and Pienza, and because it is traversed by the ancient Via Francigena pilgrimage route.

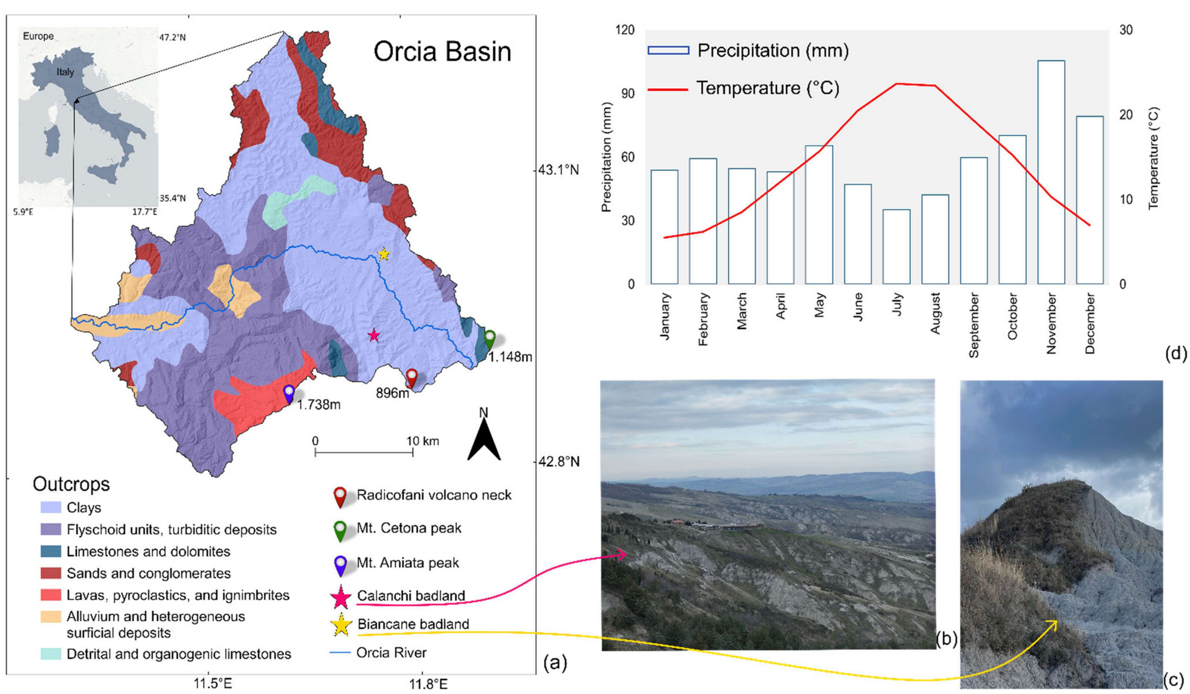

Figure 1. (a, b) Location map, outcrops, derived from Geolithological map of Italy at 1:500,000 scale (Geoportale Nazionale, Servizi WFS) and the main peak of the study area; and (c) ombrothermic diagram.

However, recent studies have demonstrated that this landscape is the product of coordinated public and private interventions throughout the 20th century, including extensive land reclamation projects and the implementation of the European Union's Common Agricultural Policy (CAP). Indeed, at the beginning of the 20th century, the landscape was considerably more barren and morphologically rugged, with sparse agricultural coverage and a widespread presence of badland landforms, resulting in an almost lunar appearance (Fresta 2011; Vergari et al. 2025). A key example of conservation efforts to preserve the remaining badland (Biancane) landforms and their associated priority habitats, which had become increasingly rare due to extensive land reclamation and still ongoing agricultural intensification, is represented by the establishment in 1996 of Lucciolabella Nature Reserve as part of the Natura 2000 network (Brandolini et al. 2018).

The climate is temperate with Mediterranean influences, characterized by dry, hot summers and wetter autumn and winter seasons (Csb – Köppen-Geiger). Average annual rainfall is approximately 726 mm/year, with peaks in November and May, while the mean annual temperature is around 14 °C.

The geological setting reflects a complex interplay of tectonics, sedimentation, and volcanism. During the Late Miocene, a major extensional phase produced NW–NW-SE-oriented horst and graben structures (Ciotoli et al., 2003). Graben sectors, such as the Radicofani Basin, in the southeastern part of the Orcia Valley, became sites of marine and lacustrine sedimentation during alternating Pliocene transgressive and regressive phases, leading to the accumulation of clays, sands, and conglomerates. In contrast, the uplifted horst blocks preserved older units, including flysch and calcareous–dolomitic formations, on which historic towns such as Pienza, Montalcino, and Castiglione d'Orcia are located. During the Quaternary, magmatic intrusions and volcanic activity associated with the Amiata and Radicofani volcanoes caused regional uplift (Acocella and Rossetti 2002; Liotta 1996), exposing Pliocene marine deposits at elevations 750–900 m a.s.l. (Figure 1b) The Radicofani volcano is now represented only by its neck, a prominent morphological landmark formed by erosion-resistant trachybasaltic lavas. The ridge connecting Mt. Amiata, Radicofani, and Mt. Cetona forms a watershed divide between the Ombrone River basin to the north and the Tiber River basin to the southeast.

The most geomorphologically active areas in the Upper Orcia Valley are associated with clay-rich soils, particularly on steep slopes (Figure 1a). Locally known as *Calanchi* and *Biancane*, these erosional landforms, which emerge on Plio–Pleistocene clays, represent distinctive badland features that form an integral part of the area's scientific and cultural heritage. These peculiar erosion landforms have developed primarily because of soil degradation processes made by man, such as deforestation, since they emerge in areas where vegetation growth is not limited by water availability, but rather by long-standing anthropogenic pressures (Gallart et al. 2013). *Biancane* are dome-shaped landforms, up to approximately 15 m high, typically found within the smoother hilly hillslopes. They are generally devoid of vegetation on their steeper, south-facing slopes, where intense erosion occurs. Despite their prevalence in the past, many *Biancane* have been levelled over the centuries due to agricultural practices aimed at increasing arable land. *Calanchi*, on the other hand, are erosional landforms that dominate the roughest and steepest sectors of the landscape, where slopes are often too steep to support human activity. They are characterized by networks of rills and gullies separated by narrow, sharp ridges and are particularly prone to mass movements, including rotational slides and complex landslides, which, together with overland flow erosion, contribute to slope denudation (Del Monte 2017; Kašanin-Grubin et al. 2018). In *Calanchi* areas, various interventions have also been implemented to reduce erosion rates and stabilize slopes (Vergari 2025).

2.2. Datasets and preprocessing

Several remote sensing and local datasets were utilized in this study to investigate trends in vegetation cover and associated environmental dynamics. Table 1 summarizes the characteristics of the remote sensing datasets, such as temporal coverage and spatial resolution, while Table 2 provides information regarding the ground-based meteorological station records, obtained from *"Servizio Idrologico Regionale della Toscana"* (Regione Toscana - Servizio Idrologico Regionale – portale SIR). Some ground-based meteorological stations provided both precipitation and temperature records, while others supplied only precipitation data.

Table 1. The remote sensing dataset used in the study, including remote sensing products, temporal coverage, spatial resolution, and their specific purpose.

Product Last accessed on 28 April 2025	Temporal coverage	Spatial resolution	Temporal resolution	# of images	Purpose in the study
Satellite data					
LANDSAT 5 ee.ImageCollection (“LANDSAT/LT05/C02/T1_L2”)	1984–2011	30 m	~16 days	2374	NDVI computation and pixel-wise quality filtering
LANDSAT 8 ee.ImageCollection (“LANDSAT/LC08/C02/T1_L2”)	2013–2021				
LANDSAT 9 ee.ImageCollection (“LANDSAT/LC09/C02/T1_L2”)	2022–2023				
MODIS LST_Day ee.ImageCollection (“MODIS/061/MOD21C3”)	2004–2023	$0.05° \times 0.05°$	Monthly	240	Temperature trend analysis and Pearson's correlation with MODIS-NDVI
MODIS LST_Night ee.ImageCollection (“MODIS/061/MOD21C3”)				240	
Global precipitation measurement ee.ImageCollection ('NASA/GPM_L3/IMERG_MONTHLY_V07')	2004–2023	$0.1° \times 0.1°$	Monthly	240	Precipitation trend analysis and Pearson's correlation with MODIS-NDVI
MODIS NDVI	2000–2023	250m	Monthly	288	Pearson's correlation analysis with LST and GPM
Use and land cover map (UCS) Tuscany Region (REGIONE TOSCANA – “Uso e Copertura del suolo - Scala 1:25.000 - Anno 1978”)	1980	1:25,000	Single	1	Analysis of LULC change
Use and land cover map (UCS) Tuscany Region (REGIONE TOSCANA - “Uso e copertura del suolo 2007-2019”)	2007–2010–2013–2016–2019	1:10,000	Single	5	

Table 2. Dataset from ground-based meteorological station used in the study, including station names, temporal coverage, altitude, and specific role in the analysis.

Station name	Geographic coordinate (WGS84[°])	Temporal coverage	Altitude (m a.s.l.)	Purpose of the study
Ground-based meteorological station.data				
a. Montenero	a. Lat 42.951, Lon 11.439	2004–2023	a. 193.00	a. Precipitation and Temperature trend analysis
b. Ripa d'Orcia	b. Lat 43.027, Lon 11.582		b. 506.00	b. Precipitation and Temperature trend analysis
c. La Foce	c. Lat 43.024, Lon 11.780		c. 563.00	c. Precipitation trend analysis
d. Montalcino	d. Lat 43.050, Lon 11.491		d. 594.00	d. Precipitation trend analysis
e. Radicofani	e. Lat 42.948, Lon 11.733		e. 618.00	e. Precipitation and Temperature trend analysis
f. Spineta	f. Lat 42.951, Lon 11.853		f. 633.00	f. Precipitation trend analysis
g. Castiglione d'Orcia	g. Lat 42.961, Lon 11.618		g. 672.00	g. Precipitation and Temperature trend analysis
h. Vivo d'Orcia	h. Lat 42.935, Lon 11.638		h. 842.00	h. Precipitation trend analysis

An overview of the complete preprocessing and analysis workflow, including satellite product and ground-based meteorological data, is provided in Figure 2. The descriptions of the datasets utilized in the present research are also summarized in Tables 1 and 2.

2.2.1. Landsat-NDVI computation

The multitemporal NDVI computation was structured into two main steps: (i) NDVI calculation and pixel-quality filtering; (ii) NDVI image mosaicking. In Google Earth Engine, monthly NDVI values from 1984 to 2023 were computed using the standard formula ($NDVI = (NIR - Red)/(NIR + Red)$), while the corresponding Pixel Quality Assessment (PQA) band was simultaneously extracted. The analysis integrated data from multiple Landsat missions, so the specific spectral bands used for NDVI calculation varied according to the sensor configuration: Landsat 5 used band 4 (NIR) and band 3 (Red), whereas Landsat 8 and 9 used band 5

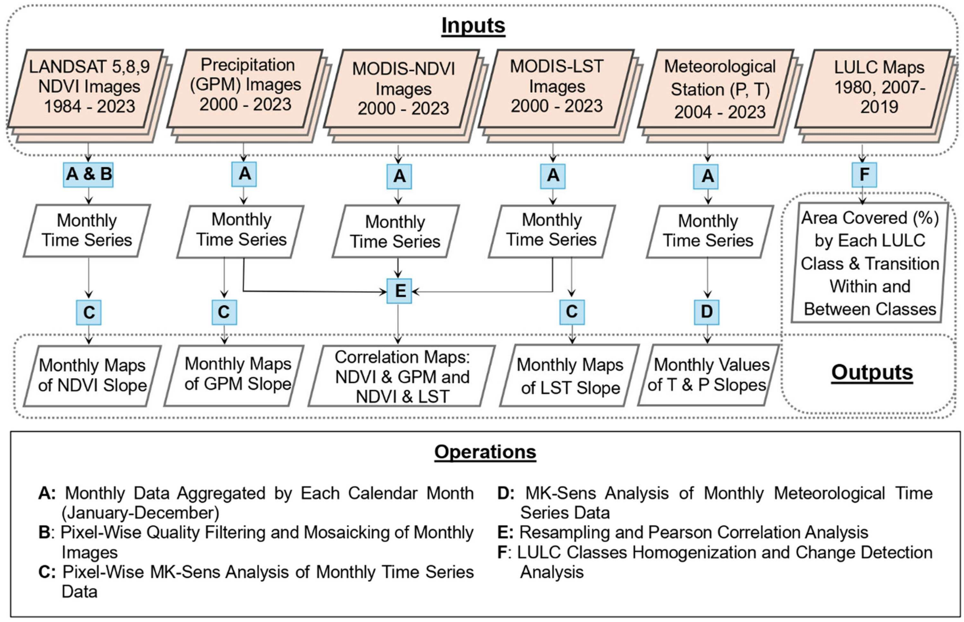

Figure 2. Workflow of the data processing and analysis steps.

(NIR) and band 4 (Red) (U.S. Geological Survey 2023; U.S. Geological Survey 2024). Since all images were sourced from the same Landsat Collection 2 Level-2 products in Google Earth Engine, which already apply consistent corrections across sensors, such as radiometric and geometric corrections, no additional cross-sensor radiometric harmonization was performed (Crawford et al. 2023).

The PQA band provides information on pixel quality regarding potential noise sources such as clouds, snow, and other atmospheric conditions (U.S. Geological Survey 2023). This information was used to filter NDVI images, retaining only valid pixels based on the general climatic conditions of the area and following the approach proposed by Ghaderpour and Vujadinovic (2020). Specifically, for Landsat 8–9, only pixels with Pixel Value 21,824, 21,826, 21,890, 22,080, 23,888, 30,048, 54,596, and 54,852 were considered valid, whereas for Landsat 5, with Pixel Value 5440, 5442, 5696, and 13,664 were retained. All pixels not matching these codes were excluded from the analysis. In cases where two Landsat images were available for the same month (due to the satellite's 16-day revisit period), a composite NDVI image was generated by applying a pixel-wise PQA-based filtering procedure. The following rules were applied: (i) if both corresponding pixels in the two images were flagged as invalid, the resulting composite pixel was marked as no data; (ii) if only one of the two pixels was valid, that value was retained in the composite image; (iii) if both pixels were valid, the one with the highest NDVI value was selected. This approach enabled the creation of monthly NDVI composites that maximize data quality and temporal continuity while minimizing the influence of atmospheric noise. In months with only one valid acquisition, the NDVI image was derived directly from that scene after PQA filtering. Due to data availability and quality constraints, not all months within the study period (1984–2023) yielded valid NDVI images. Although a theoretical total of 480 monthly images would be expected (one per month over 40 years), only 419 valid NDVI images were created. Table 3 reports the number of valid NDVI images per month.

The 107 missing images are primarily due to the lack of high-quality observations, as determined by PQA band filtering. This issue occurred mainly during autumn and winter months, when cloud cover and atmospheric disturbances are more frequent in Mediterranean regions. Additionally, the year 2012 was entirely excluded from the analysis due to the lack of operational sensors because, although several recent studies have successfully applied gap-filling approaches (Asare et al. 2020; Yin et al. 2017), such methods generally rely on auxiliary multitemporal or multisensor data and radiometric adjustment procedures that may introduce additional uncertainties, and artefacts to the time-series dataset (U.S. Geological Survey 2019). Overall, most NDVI images used in the analysis exhibit valid pixel coverage exceeding 80% (Figure 3).

Table 3. Number of NDVI images for each month.

	# of NDVI images
January	31
February	33
March	36
April	32
May	37
June	38
July	37
August	38
September	37
October	35
November	35
December	30
Total	419

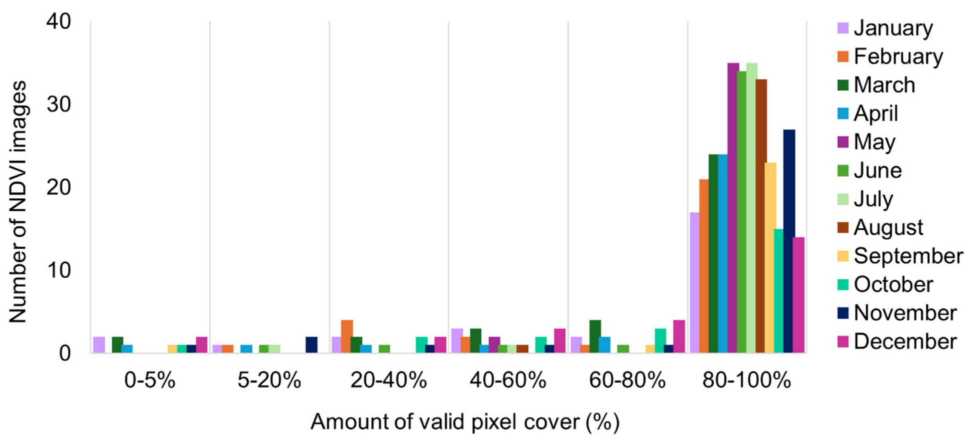

Figure 3. Distribution of valid pixel coverage in NDVI monthly images from 1984 to 2023, grouped by percentage intervals of valid pixel cover. The number of images per month is indicated in the legend.

2.2.2. Thermo-pluviometric dataset

To detect the presence of a statistical trend in climatic variables, expressed as temperature and precipitation records, two types of datasets were used. The first source consisted of ground-based meteorological station records, spread all around the study area (Table 2), from which monthly maximum (Tmax), minimum (Tmin), and mean (Tmean) air temperatures, total monthly precipitation, and precipitation intensity (defined as the ratio between total monthly rainfall and the number of rainy days) were obtained. The second source consisted of satellite-derived climatic products (Table 1): MODIS LST was used to derive monthly daytime and nighttime land surface temperatures, while GPM data were used to derive monthly precipitation totals and precipitation intensity. Moreover, the satellite-derived dataset was used to carry out the correlation analysis between vegetation and climate (see 2.3.4 MODIS NDVI-climate correlation chapter).

2.2.3. Land use and land cover (LULC) dataset

To investigate spatial and temporal changes in LULC, multiple datasets were employed: (i) the LULC map of 1980, which represents land cover conditions at the onset of the NDVI time series (1984), and (ii) a series of more recent LULC maps for 2007, 2013, 2016, and 2019, which document subsequent stages of landscape evolution up to the final part of the analysis period (2023). Since the 1980 map was originally developed using land-use designations (e.g. “Coppice forests” instead of “Broad-leaved forest”), it was harmonized with the CORINE Land Cover classification to ensure comparability with the most recent dataset (Table 4), developed according to that system. Finally, all datasets were grouped into the following categories: Artificial surfaces; Arable land; Permanent crops; Pastures; Heterogeneous agricultural areas; Broad-leaved forest; Coniferous forest; Mixed forest; Shrub and herbaceous vegetation associations; Beaches, dunes, and sand plains; Bare rock; Sparsely vegetated areas; Inland water.

Table 4. Reclassification of LULC of 1980 map into the new categories.

LULC 1	Land use units
• Quarry/extractive area	Artificial surfaces
• Urbanized area (including low-density urbanization)	
• Dry cropland (arable)	Arable land
• Irrigated cropland and/or reclaimed land	
• Chestnut orchard (for fruit production)	Permanent crops
• Specialized fruit orchard	
• Specialized olive grove	
• Specialized olive vineyard	
• Specialized vineyard	
• Nursery and greenhouse	
• Wooded pasture	Pastures
• Bare and shrub pasture	
• Meadow-pasture and permanent meadow	
• Productive fallow land	Heterogeneous agricultural areas
• Arborated cropland with fruit trees and others	
• Arborated cropland with vines	
• Arborated cropland with olives and vines	
• Arborated cropland with olives	
• Coppice woodland	Broad-leaved forest
• Coppice woodland converted to high forest or overgrown	
• High forest of broadleaf	
• Riparian, riverbank, and floodplain tree formations	
• High forest of conifers	Coniferous forest
• Mixed high forest	Mixed forest
• Poplar plantation (and other timber plantations)	Shrub and herbaceous vegetation associations
• Reforestation and young woodland	
• Watercourse and canals	Beaches, dunes, and sand plains
• Rock outcrop	Bare rock
• Denuded area with diffuse erosion	Sparsely vegetated areas
• Badland (calanco)	
• Firebreak strip and ski slope	
• Water body (lakes and artificial reservoirs)	Inland water

2.2.4. MODIS-NDVI and climate correlation analysis

To investigate the strength and direction of a linear relationship between NDVI and LST and between NDVI and GPM, Pearson's correlation analysis was conducted. Due to the coarser resolution of LST (~5.5 km) and GPM (~11 km), a monthly MODIS-NDVI composite at 250 m resolution from 2000 to 2023 was employed, as also utilized by Ghaderpour et al. (2023). The overall monthly MODIS-LST products were calculated as the average of daytime and nighttime monthly observations for each pixel (Chen et al. 2017). Since MODIS revisits the study region every day, this composite is derived from choosing the best-quality pixels that have the highest NDVI values because clouds, haze, aerosols, and poor geometry tend to decrease NDVI (Didan and Munoz 2021; Robinson et al. 2017). Since Landsat has a 16-day revisit over the study area (not daily), it captures sharper temporal changes but with sparser sampling. Therefore, MODIS-NDVI is often favored for phenology and climate–vegetation correlation analyses, while Landsat excels at spatial detail (Ghaderpour et al. 2023). Another reason for choosing MODIS NDVI over Landsat-derived NDVI is due to the lower spatial resolution of LST and GPM images; i.e. a common practice for correlation analysis is to downsample the NDVI images to match the spatial resolution of LST and GPM. So, higher spatial resolution of NDVI is not an issue for this application. Using a median approach, monthly MODIS-NDVI images are downsampled from a resolution of 250 m to match the MODIS-LST resolution (~5.5 km). This process was done in Python using the command "gdal.ReprojectImage()." Likewise, monthly MODIS-NDVI images are downsampled from a resolution of 250 m to match the GPM resolution (~11 km), using the same Python command.

2.3. Methods

2.3.1. Mann–Kendall test and Sen's slope estimator

To assess long-term trends in vegetation and climate variables, the Mann–Kendall test, associated with Sen's slope estimator (MK-Sen), was applied with a 95% confidence level. The *pyMannKendall* package was used (Hussain and Mahmud 2019). Widely employed in climate studies, the test finds trends in time-series data, with Sen's slope estimating their magnitude and direction (Ghaderpour et al. 2025; Boccolari and Malmusi, 2013; Ghaderpour et al. 2024; Karpouzos, Kavalieratou, and Babajimopoulos 2010). The mathematical specifications of the MK-Sen test are in the following works: KENDALL (1938), Mann (1975), and Sen (1968). For each calendar month, the MK-Sens test was executed to: i) monthly NDVI images; ii) precipitation and temperature datasets (derived from both satellite products and ground-based meteorological stations). Moreover, the NDVI data were analyzed over three temporal windows: the full observation period (1984–2023), the first 20-year interval (1984–2003), and the second 20-year interval (2004–2023). Precipitation and temperature trends were examined only for the most recent 20-year period (2004–2023) to enable a consistent comparison with NDVI trends over the same period. To facilitate the interpretation of Sen's slope values, results were classified into eight discrete classes (Table 5) as proposed by Ghaderpour et al. (2023), and the values were reported as percentage cover by each class.

For the trend analyses based on satellite imagery (Landsat-NDVI, LST daytime, LST nighttime, GPM), results were also expressed as the area covered by pixels showing statistically significant trends, in order to quantify how spatially extensive these changes were across the study region.

2.3.2. LULC change detection

To evaluate the presence and effects of LULC change on vegetation and badlands dynamics, a percentage-based comparison was carried out on the extent of each LULC class between 1980 and 2019. Only comparing 1980 with 2019, a binary change map was produced to classify the study area into two categories: changed and unchanged LULC. This binary map was then spatially overlaid with the distribution of monthly NDVI data to determine whether NDVI variations were more concentrated in areas affected by land-use and land-cover change. Finally, for areas identified as affected by LULC change according to the binary map, a transition matrix was generated to identify the direction of change, i.e. whether an area changed within the same land-cover categories (e.g. from arable to pastures) or transitioned to a different one (e.g. from arable to mixed forest), to obtain more in-depth information about the specific pathways of change, thus offering a more process-oriented interpretation of landscape evolution.

3. Results

3.1. Landsat-NDVI analysis

The MK-Sen test on monthly NDVI imagery shows a general greening trend across the study area during the full observation period, with most pixels showing an increase of approximately 0.005 units per year, followed by less widespread but more pronounced increases of 0.010 units per year. Negative trends were detected too, although they were limited in spatial extent and typically around −0.005 units per year. The highest slope values were observed along river courses: the riverbed of the Orcia River in the middle and lower Orcia Valley, as well as its tributary Formone Stream in the Upper Orcia Valley, showed changes, with slope values ranging from 0.005 to 0.015 units per year. These trends can be attributed to the expansion of riparian vegetation along the watercourses, primarily consisting of trees, shrubs, and undergrowth. A greening trend was also evidenced in the badlands area (Upper Orcia Valley), which may have influenced river morphodynamics. A reduction in sediment supplies due to hillslope-scale modifications such as land-use change processes can trigger river transitions from braided systems to single channels, leading to the stabilization of formerly active channels, where riparian vegetation can grow easily. Figure 4 shows the results of the NDVI trend analysis over the entire study period (1984-2023), illustrating the percentage of each slope class relative to the total basin area. The months that recorded an NDVI increase were those of the vegetation growing season (May–October), while variations were negligible during the winter months, except for a slight increase detected in March.

When the trend is analyzed separately for the 1984–2003 and 2003–2024 periods, they reveal contrasting patterns. During the first analysis period (1984–2003), most of the study area did not experience significant NDVI changes (Figure 5). However, where changes were found, they were mostly associated with negative

Table 5. Classification of slope values into eight classes based on slope gradient intervals.

Class 1	Class 2	Class 3	Class 4	Class 5	Class 6	Class 7	Class 8
slope < −0.0-15	−0.015 ≤ slope < −0.010	−0.010 ≤ slope < −0.005	−0.005 ≤ slope < 0	0 ≤ slope < 0.005	0.005 ≤ slope < 0.010	0.010 ≤ slope < 0.015	Slope ≥ 0.0-15

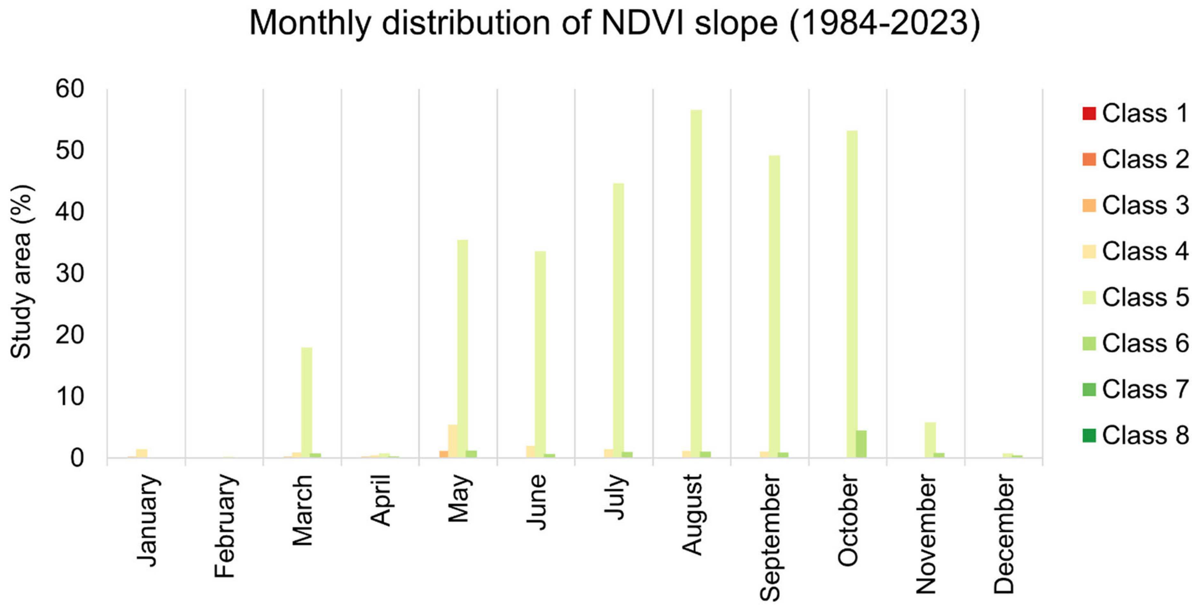

Figure 4. Monthly distribution of NDVI trend slope classes over the study area from 1984 to 2023. The bars represent the percentage of the study area falling into each NDVI slope class for each month.

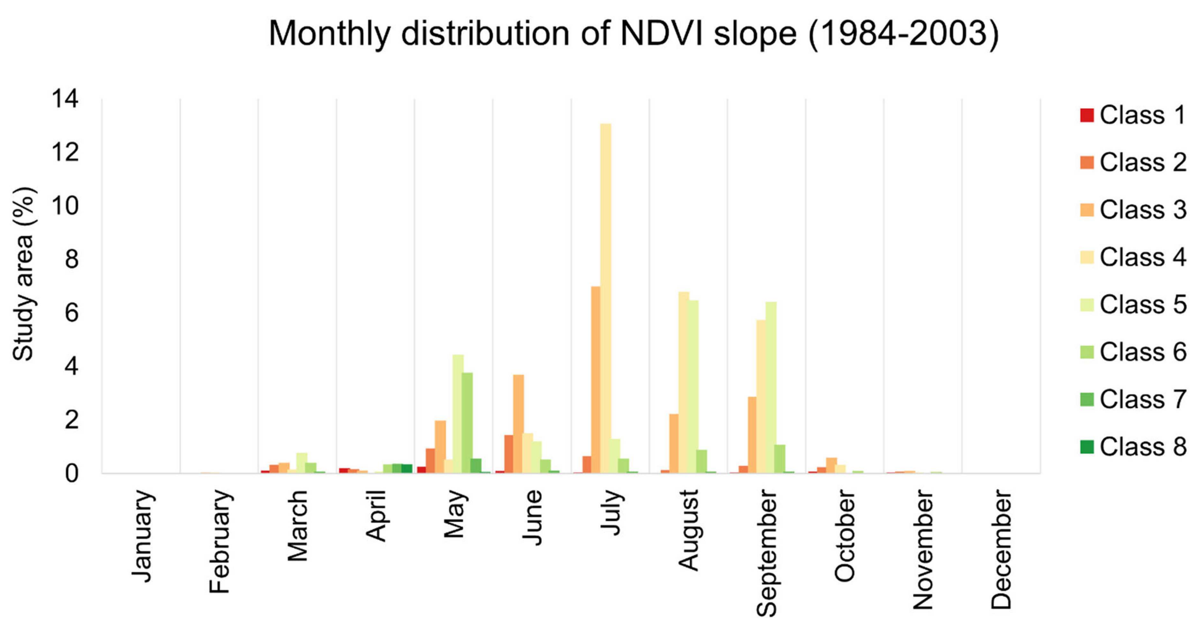

Figure 5. Monthly distribution of NDVI trend slope classes over the study area from 1984 to 2003. The bars represent the percentage of the study area falling into each NDVI slope class for each month.

trends. In particular, the spring–summer months were characterized by a slight decrease in NDVI, with trends typically around −0.005 NDVI units per year.

Finally, during the most recent period (2004–2023), NDVI trends indicate a positive increase that is spatially more widespread and more intense compared to the 1984–2003 period (Figure 6). In this period, the velocity of change is more intense, ranging from 0.005 to 0.010 NDVI units per year. Notably, even the winter months exhibited non-negligible NDVI increases, largely driven by contributions from higher slope classes, corresponding to 0.010 to 0.015 NDVI units per year, indicating a faster rate of increase during this period.

3.2. Thermo-pluviometric trend results

3.2.1. Trend results of the temperature time series

The MK-Sen test performed at a 95% confidence level detected significant warming signals in both the LST and ground-based meteorological stations dataset. LST results (Table 6) indicate stronger and more widespread nocturnal than diurnal warming, with the most extensive signals in summer (e.g. July and August: >80% of the basin affected, slopes of 0.08–0.18 °C/year) and in winter (e.g. December and February). A limited nocturnal cooling trend was detected in April (slope ≈ −0.10 °C/year). The spatial distribution of positive slopes indicates a clear seasonal pattern, with the largest areas affected by warming during summer months and secondary peaks in late winter. These results are consistent with those from ground-based meteorological stations (Table 7), which show the strongest warming signals in summer, especially for minimum and mean temperatures (0.08–0.21 °C/year). A clear warming signal is also evident in December and February, the latter in agreement with the LST results. Finally, it must be noted that when the temperature trend analysis is performed over a 30-year timespan (for data from ground-based

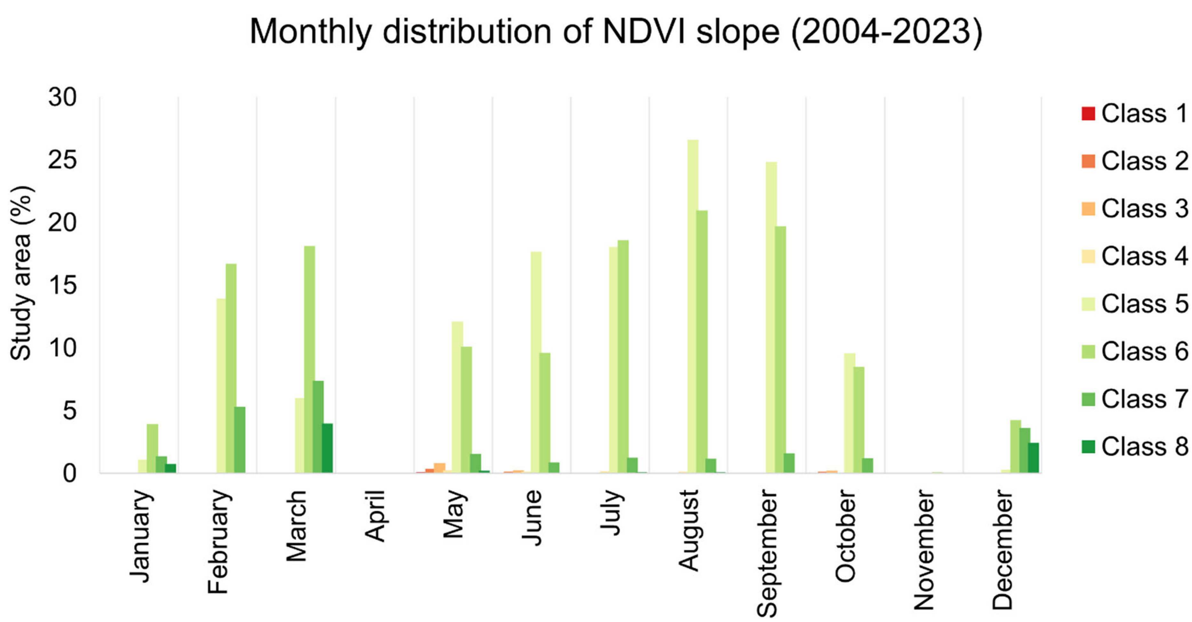

Figure 6. Monthly distribution of NDVI trend slope classes over the study area from 2004 to 2023. The bars represent the percentage of the study area falling into each NDVI slope class for each month.

Table 6. Monthly distribution of the affected area (%) and corresponding slope ranges for day- and night-time land surface temperature (LST) trends. Values refer to the proportion of the study area showing significant temperature trends between 2004 and 2023. Only months and variables showing a significant trend are reported.

	Area affected day	Area affected night	Slope range day	Slope range night
January				
February	16.94%	25.41%	0.16–0.21	0.15–0.20
March	5.64%		0.10–0.12	
April		2.82%		−0.10
May				
June		5.64%		0.12
July		81.89%		0.08–0.14
August		84.71%		0.11–0.18
September				
October				
November		14.11%		0.05–0.08
December	3.33%	100%	0.12–0.17	0.13–0.20

Table 7. Monthly slope values of temperature trends (Tmax, Tmin, and Tmean) measured at four ground-based meteorological stations from 2004 to 2023. Only significant trends (*p* value 0.05%) are reported, and values represent the rate of change in °C per year (slope of MK test).

	Montenero			Ripa d'Orcia			Radicofani			Castiglione d'Orcia		
	Tmax	Tmin	Tmean	Tmax	Tmin	Tmean	Tmax	Tmin	Tmean	Tmax	Tmin	Tmean
January												
February	0.20			0.18			0.21		0.18			
March	0.11		0.11				0.15		0.10			
April												
May		0.12										
June		0.15	0.12		0.15			0.12	0.12		0.14	
July		0.18	0.12		0.11	0.08	0.13	0.11	0.11			
August	0.18	0.14	0.14	0.13	0.12	0.13	0.21		0.17	0.13		0.11
September		0.11	0.11		0.10		0.14					
October	0.14		0.08				0.13					
November		0.15	0.11		0.11						0.08	
December	0.16	0.10	0.14	0.13	0.15	0.13	0.15	0.15	0.13	0.14	0.12	0.14

Table 8. Monthly slope values of precipitation trends (monthly trend and intensity) measured at three ground-based meteorological stations of eight, from 2004 to 2023. Only significant trends (*p* value 0.05%) are reported, values represent the rate of change in °C per year (slope of MK test).

	Montalcino		Radicofani		Castiglione d'Orcia	
	Monthly trend	Intensity trend	Monthly trend	Intensity trend	Monthly trend	Intensity trend
January						
February						
March						
April		0.22	1.82			
May		−0.25				
June						
July	1.92					0.32
August						
September						
October						
November						
December						

meteorological stations), the magnitude of change (slope) decreases by one order of magnitude in most cases.

3.2.2. Trend results of precipitation time series

The MK-Sen test performed at a 95% confidence level did not detect any statistically significant general trend in either GPM or ground-based meteorological data. GPM analysis did not reveal any significant trends over the study period, while ground-based station data showed localized and seasonally limited variations (Table 8). Positive trends in monthly total precipitation were detected at Radicofani in April and at Montalcino in July, while increases in precipitation intensity were detected at Montalcino in April and at Castiglione d'Orcia in July. A slight decrease in intensity was recorded at Montalcino in May.

3.3. LULC change multitemporal pattern

In 1980, the study area was predominantly covered by agricultural surfaces (Figure 7). Arable land dominated the central zone, forming a continuous belt extending from the north-central sector toward the eastern and southeastern flanks. Permanent crops and pastures, although more scattered, were interspersed within this matrix, particularly near the transition zones toward the hillier western and southern margins. Agricultural areas in the eastern and southern sectors were more fragmented and mixed with natural or semi-natural vegetation, likely due to steeper slopes and more articulated topography. Forests were mainly concentrated along the western and southern ridges' slopes, while smaller and more fragmented patches occurred along the northeastern and southeastern borders. In the same sector, sparsely vegetated areas, including pasture surfaces and badlands landforms, were concentrated on the steeper slopes of the upper Orcia Valley, indicating erosion-prone zones as documented in previous studies (Ciccacci et al. 2008; Aucelli et al. 2014; Vergari et al. 2019). Artificial surfaces occupied only a small portion

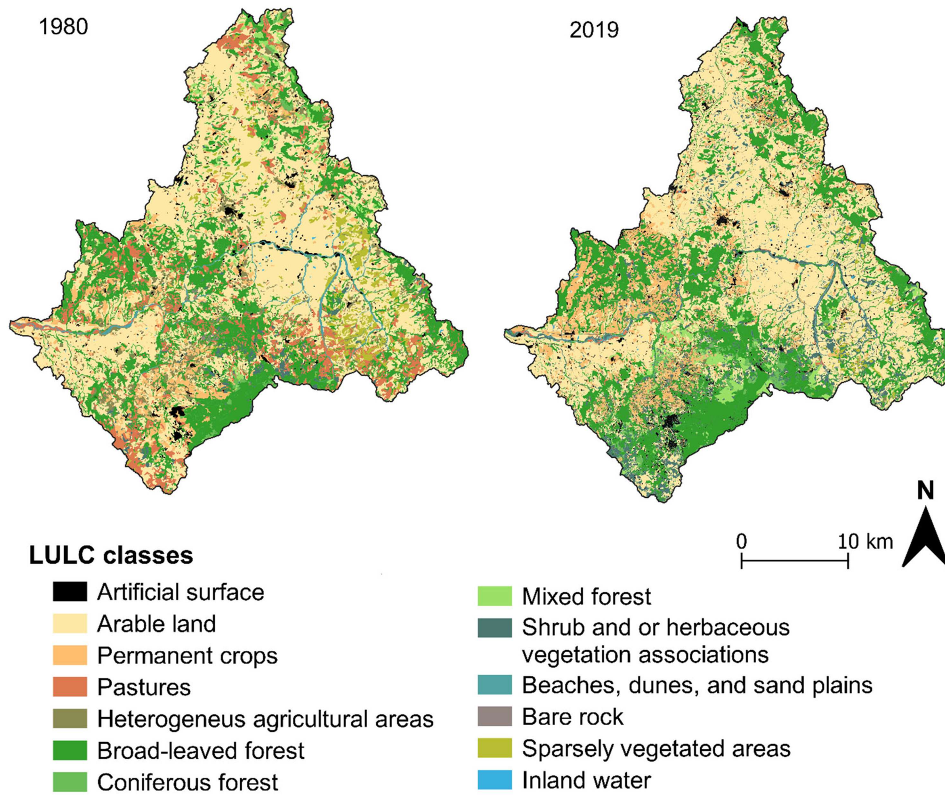

Figure 7. LULC maps of the study area for the periods 1980 and 2019.

of the landscape, mainly corresponding to historical settlements and riverbed mining areas along the middle course of the Orcia River.

From 2007 onwards, the agricultural belt is still clearly visible, and this category continues to represent the predominant LULC class. However, several changes occurred (Figure 7): (i) the western sector experienced an increase in permanent crops, replacing former arable and pasture areas; (ii) the south–southwestern sector showed a marked expansion of forest cover, as did the southern and eastern borders of the study area; (iii) sparsely vegetated areas were almost entirely converted into agricultural land or recolonized by forest vegetation; and (iv) artificial surfaces previously observed along the Orcia River were no longer visible, supporting the hypothesis that riverbed extraction activities had ceased. Thus, between 1980 and 2019, 42% of the study area was affected by land-use changes, while 58% remained stable (Figure 8). Table 9 reports the percentage variation for each LULC class between 1980 and 2019. The main land use changes were registered between 1980 and 2007. The pronounced decline in sparsely vegetated areas provides straightforward evidence of badlands reduction.

The overlap between the NDVI variation (1984–2023) maps and the binary LULC change map (Figure 8a) revealed a general predominance of NDVI changes occurring in areas that had undergone land-use transitions, even though the extent of these areas was smaller than that of stable LULC (Figure 8b). Specifically, during late spring, summer, and early autumn, the percentage of NDVI pixels in changed areas exceeded that of stable areas, whereas during the winter months and early spring, the percentages remained similar across both categories, indicating limited vegetation activity regardless of land-cover status. Examples of NDVI multitemporal trends in areas affected by both stable LULC and LULC change are shown in Figure 9. Indeed, a substantial proportion of pixels exhibiting NDVI variations fall within areas of stable LULC, indicating that secondary processes, such as coppice land abandonment, may contribute to the changes in vegetation index values.

Table 10 reports the transition matrix among classes affected by LULC changes according to the binary map. Considering the agricultural categories (Arable lands, Permanent crops, Pastures, and Heterogeneous agricultural areas), internal reorganization accounts for 34.98% of the total land cover changes in the area.

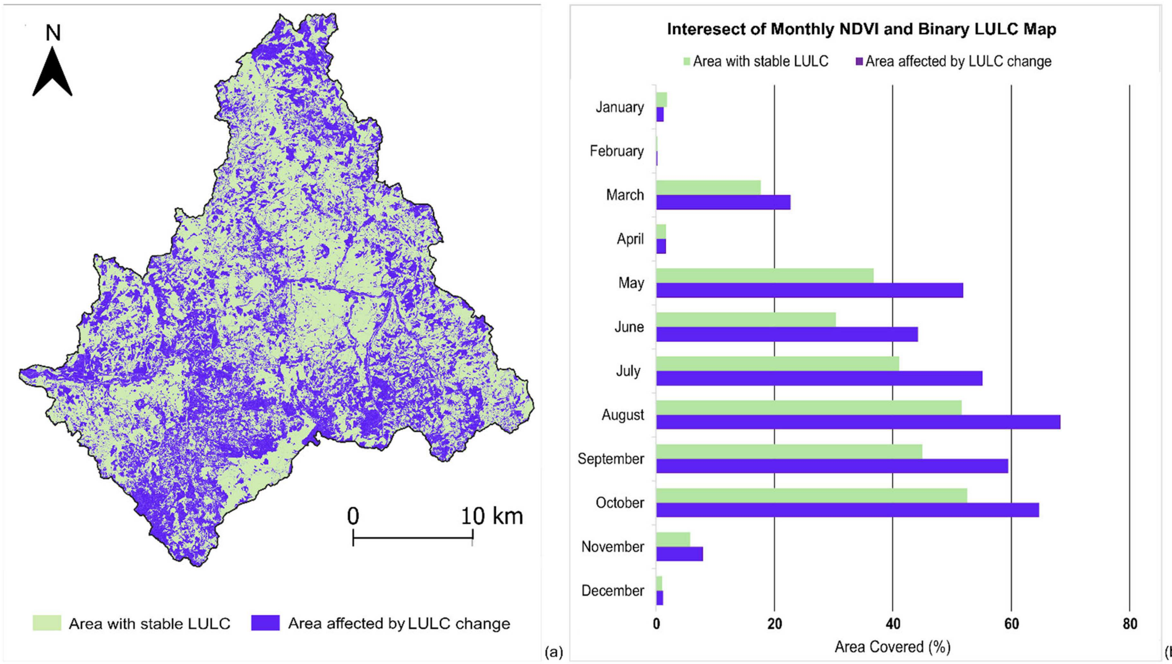

Figure 8. (a) Binary map of areas affected and unaffected by LULC changes (1980–2019). (b) Intersection between LULC binary classes and monthly NDVI variation data.

Table 9. Percentage of total area occupied by each LULC class in the time periods and the absolute change (Δ%). Positive values indicate expansion, while negative values indicate a reduction in area.

LULC classes (%)	LULC 1980	LULC 2007	LULC 2010	LULC 2013	LULC 2016	LULC 2019	Δ UCS2019–UCS1980
Artificial surface	1.70	4.35	4.33	4.34	4.36	4.40	+2.70
Arable land	42.90	42.75	42.44	42.22	42.13	41.62	−1.28
Permanent crops	6.96	10.21	10.50	10.59	10.64	11.04	+4.08
Pastures	8.89	0.65	0.70	0.78	0.80	0.79	−8.10
Heterogeneous agricultural areas	6.17	1.44	1.42	1.40	1.42	1.41	−4.75
Broad-leaved forest	24.59	29.01	29.03	29.03	29.04	29.06	+4.47
Coniferous forest	0.70	1.58	1.56	1.54	1.53	1.53	+0.83
Mixed forest	1.40	2.22	2.22	2.22	2.21	2.22	+0.82
Shrub and/or herbaceous vegetation associations	1.24	6.60	6.61	6.61	6.60	6.68	+5.45
Beaches, dunes, and sand plains	1.23	0.22	0.24	0.29	0.29	0.25	−0.98
Bare rock	0.30	0.08	0.08	0.08	0.08	0.09	−0.21
Sparsely vegetated areas	3.79	0.69	0.69	0.70	0.69	0.69	−3.10
Inland water	0.09	0.18	0.19	0.19	0.20	0.20	+0.11
Non-photointerpretable area	0.04						
Total	100.00	100.00	100.00	100.00	100.00	100.00	

The major increasing agricultural category is the Permanent crops (16.17% of the total changed area), which may indicate a growing valorization of typical products: the expansion of vineyards and olive groves often reflects the growth of the quality wine, tourism, and agri-food sectors. Conversely, 33.17% of the changed areas represent a transition from agricultural to non-agricultural land cover classes; the most frequent destination class was Broad-leaved forest (15.77%), which may reflect land abandonment processes. Forest-related categories (Broad-leaved, Coniferous, and Mixed forests) experienced 8.73% of transitions to other macro-categories (agricultural or shrub/herbaceous areas) and 7.94% of internal transitions. The latter were mainly directed towards an increase in Broad-leaved forest (3.81%), while the most frequent conversions from forest areas were toward Arable land (3.83%). This pattern may indicate cessation of coppice management in the first case and localized deforestation for agricultural purposes in the second. The category Shrub and/or herbaceous vegetation associations primarily underwent transitions towards Coniferous forest areas, suggesting a localized afforestation action. Considering the categories Beaches, dunes and sand plains, and Bare rock, only the first one experienced a category change, which may indicate

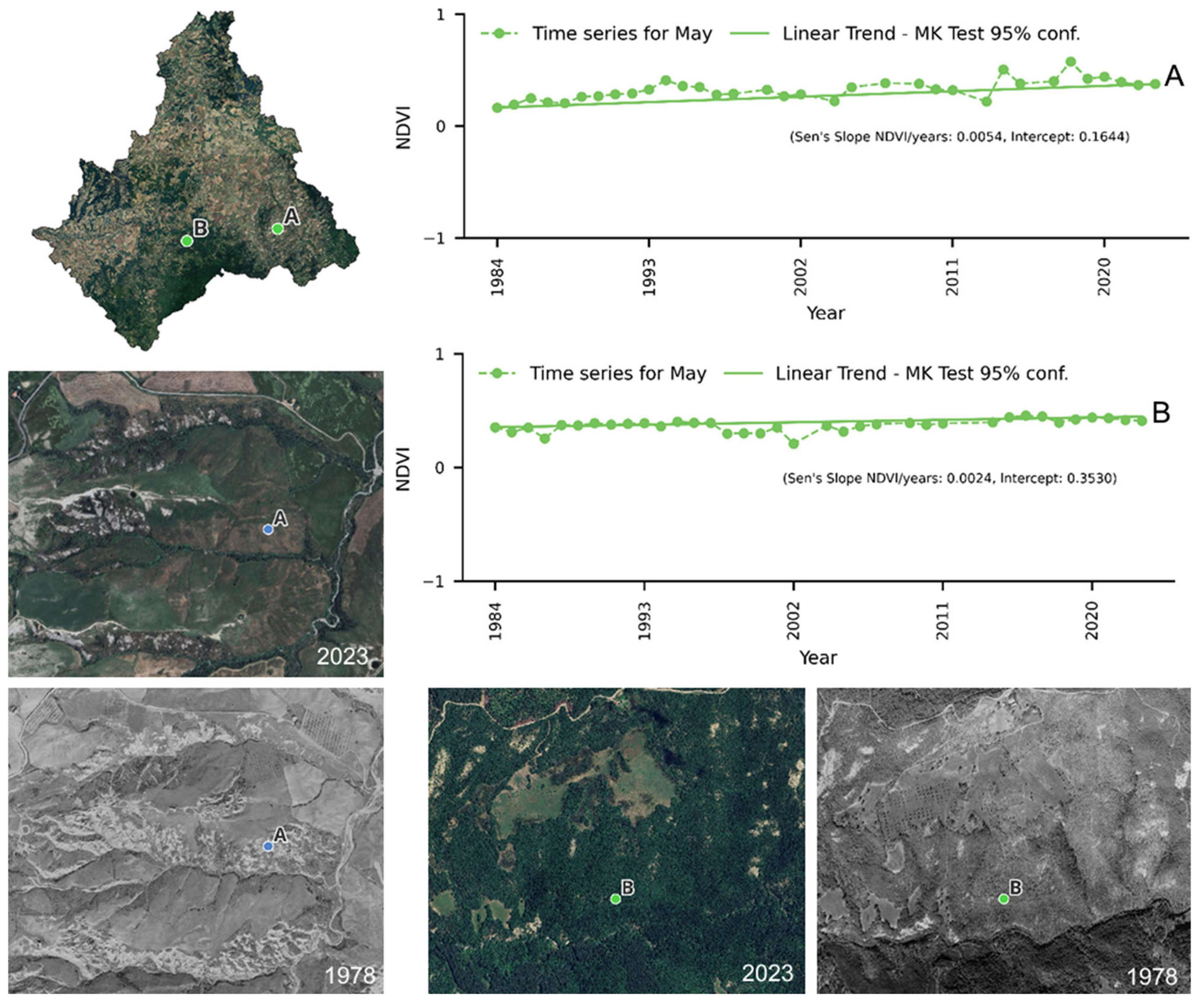

Figure 9. Examples of areas with increased NDVI in May. Trend in (A) illustrates a site where the increase coincided with a LULC change from Badlands to agricultural land. Trend in (B) shows a site with stable LULC, remaining classified as broad-leaved forest throughout the period. Background images derived from a historical aerial photo for 1978 and a basemap in QGIS.

a natural stabilization and vegetation recovery of formerly bare/unstable surfaces. Sparsely vegetated areas, which this study associated mainly with badlands landforms, account for 6.16% of category changes. The dominant destination class was Arable land, followed by Shrubs and or vegetation associated. This pattern clearly reflects both the practice of reclaiming badlands for agricultural purposes and the abandonment of traditional agricultural activities such as grazing (which play a crucial role in the badlands development), and the consequent natural vegetation recovery, suggesting the potential disappearance of badlands. Artificial surfaces also emerged as a recurrent destination class, receiving transitions from nearly all land-cover types, although these transitions remain relatively limited in absolute terms.

3.4. MODIS-NDVI and climate correlation results

Figure 10 shows the Pearson's correlation maps between NDVI and LST and between NDVI and GPM. Each pixel value is estimated from 288 pairs of NDVI and LST or NDVI and GPM values (24 years from 2000 to 2023 multiplied by 12 months) as described in Ghaderpour et al. (2023).

Figure 10(a) shows that most of the study area exhibits weak Pearson's correlation coefficients between NDVI and LST, with values generally ranging between −0.3 and 0.3, while moderate to high positive correlations are mostly confined to the southern sector and, in general, where broadleaf forests dominate. Figure 10(b) indicates predominantly weak correlations between NDVI and precipitation, with values mainly

Table 10. Transition matrix for classes affected by land-use change (based on the binary map), showing the direction of change in terms of % of the total changed areas.

TRANSITION MATRIX(%)		LULC 2019 Artificial surface	Arable land	Permanent crops	Pastures	Heterogeneous agric. area	Broad-leaved forest	Coniferous forest	Mixed forest	Shrub and or herb. veg. ass.	Beach. dunes and sand plain.	Bare rock	Sparsely veg. areas	Inland water
LULC 1980	Artificial surface		0.48	0.31	<0.1%	0.12	0.27	–	–	0.37	–	–	<0.1%	–
	Arable land	4.05		9.7	<1%	0.90	5.73	0.32	0.30	3.83	–	0.1	0.1	0.2
	Permanent crops	0.98	2.29		<1%	0.62	3.62	0.12	0.24	0.51	–	–	<0.1%	–
	Pastures	0.69	7.36	1.80		0.35	4.58	0.58	0.63	4.27	–	0.1	0.1	–
	Heterogeneous. agric.area	0.85	4.47	4.66	0.17		1.85	–	0.14	1.02	–	–	<0.1%	–
	Broad-leaved forest	1.05	3.62	1.34	0.18	0.17		1.03	2.76	1.60	0.1	–	0.1	–
	Coniferous forest	–	–	–	–	–	1.01		0.33	–				–
	Mixed forest	–	0.16	–	–	–	2.80	–		–	–		–	–
	Shrub and or herb. veg. ass	–	0.10	–	–	–	0.60	1.29	0.51		–	–	–	–
	Beach. dunes and sand plain	–	0.27	–	–	–	0.68	–	–	1.34	–	–	–	–
	Bare rock	–	–	–	–	–	0.26	–	–	<1%	<1%		–	–
	Sparsely veg. areas	0.12	3.99	–	–	–	0.98	–	–	2.16	<1%	<1%		–
	Inland water	–	–	–	–	–	–			–				
	Total	7.9	22.9	18	1.4	2.2	22.4	3.5	5.0	15.4	0.2	0.1	0.3	0.4

– = <0,01%

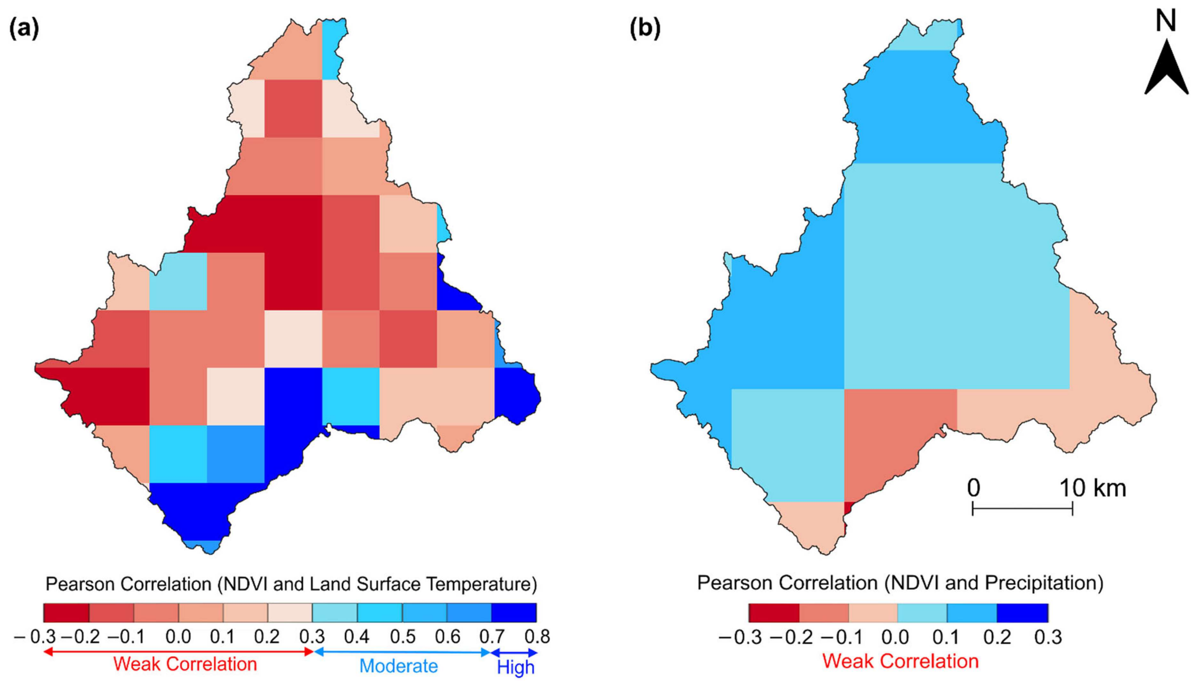

Figure 10. The Pearson's correlation maps for (a) NDVI and LST, and (b) NDVI and precipitation (GPM), estimated from monthly images from 2000 to 2023.

between −0.2 and 0.2, and only a slight tendency towards negative coefficients in the more forested southern part of the region.

4. Discussion

4.1. Comparison with literature

The NDVI analysis from 1984 to 2023 revealed a clear greening trend across the study area, likely contributing to the decline of badland surfaces. This greening trend is supported by the use of the non-parametric Mann–Kendall test, which detects the presence of statistically significant monotonic trends over time. Consequently, the values presented do not correspond to the NDVI itself but to the slope of its trend, reflecting the rate and direction of vegetation change. The marked positive slopes observed, particularly between May and October, therefore suggest that the badland areas are undergoing a progressive revegetation process, consistent with the overall trend observed across the catchment.

Over the entire analyzed period, NDVI trends point to a gradual greening, with positive changes concentrated in the months from May to October and no evidence of widespread negative trends. In particular, the persistence of higher NDVI values into October may reflect a delayed onset of vegetation senescence and a prolongation of the growing season beyond the conventional late-September limit. This behavior can be explained by both changes in land-use practices, such as the expansion of irrigated crops and the introduction of more sophisticated water-management systems, and by relatively mild autumn temperatures and/or moderate September–October rainfall that help maintain active vegetation cover. In the first two decades (1984–2003), NDVI trends show only limited changes, with summer dominated by negative slopes that are consistent with crop harvesting, grazing, and the typical summer drought response of Mediterranean vegetation. By contrast, the signal becomes clearly more positive and spread in the more recent part of the record (2004–2023), with a marked increase in NDVI in the majority of the months, indicating a clear shift in vegetation dynamics.

The increases in vegetation coincided with changes in climatic conditions and land cover, suggesting synergistic effects from multiple drivers.

The trend analyses applied separately to NDVI and temperature datasets both indicated increasing trends over the 2004–2023 period (Figure 6; Tables 6 and 7). The most notable increases in NDVI occurred during months with the highest positive temperature trends, especially in late winter and summer. Warmer winter and early spring temperatures may reduce cold stress and encourage earlier greening. Indeed, this pattern suggests decreased thermal seasonality, a possible decline in winter stress for vegetation, and a prolonged and warmer summer thermal regime. Recent research on climate change impacts on vegetation indicates that moderate warming can prolong the growing season and boost plant productivity, a process also supported by the fertilizing effect of CO_2. However, these advantages occur only where water availability remains sufficient (Cannone, Sgorbati, and Guglielmin 2007; Maselli 2004; Chelli et al. 2017; Bellini et al. 2023; Fibbi et al. 2019). Since our study showed a stable rainfall pattern, and some meteorological stations even recorded increases in both the amount and intensity of monthly rainfall, we can infer that warming conditions, coupled with no increase in drought, have consistently driven the changes in vegetation observed during the second study period (2004–2023). Indeed, localized rainfall increases during spring and summer could have improved soil moisture availability and enhanced vegetation productivity, partially mitigating thermal and drought stress in recent years. Finally, the analysis of climatic trends, which revealed a significant increase in temperature and a non-significant trend in precipitation, is consistent with the findings of Giaccone et al. (2015), who examined the evolution of these climatic variables over the period 1965–2012 in the study area.

The Pearson correlation analysis between MODIS-derived NDVI and LST and between MODIS-derived NDVI and GPM indicates predominantly weak linear relationships, with most coefficients falling within ranges typically classified as low (Ratner 2009). This pattern is consistent with Mediterranean environments (Ghaderpour et al. 2023), where NDVI usually attains its highest values in spring and early summer and declines towards late summer, whereas precipitation tends to be highest during late autumn and winter and lowest in mid-summer; such phase mismatches between vegetation activity and rainfall tend to flatten the overall correlations when assessed at the annual scale. The weakly negative NDVI–precipitation coefficients in the southern, more forested sector reflect a seasonal regime in which vegetation reaches maximum activity in late spring while precipitation is already decreasing. In other parts of the study area, rainfall is rapidly converted into surface runoff over crusted, low-permeability (often clayey) surfaces, reducing its effectiveness in sustaining vegetation growth and further contributing to the generally weak correlations revealed by the Pearson analysis.

The increase in vegetation aligns with land-use transformations observed between 1980 and 2019 (Table 9; Figure 7), which showed the expansion of permanent crops, broad-leaved forests, and shrub or herbaceous formations, alongside a marked decline in pastures, heterogeneous agricultural areas, and sparsely vegetated zones, including badlands. The landscape appears to be following a dual trajectory in which forest expansion driven by land abandonment coexists with agricultural intensification, primarily through the growth of arable land and permanent crops. This pattern indicates a progressive contraction of open and degraded environments in favor of denser and more persistent vegetation cover and reflects a shift from diversified, often extensive agro-farming systems toward a more specialized and intensive agricultural model, in which the conversion of badland landforms into arable land and the spread of high-value permanent crops such as olive groves highlight the persistent human pressure to reclaim and reshape highly erodible terrains.

Similar greening trends have been reported throughout the Mediterranean basin, where climatic and land-use factors, acting alone or together, are commonly cited to explain NDVI increases. For instance, Ghaderpour et al. (2023) documented steady NDVI growth across the Italian peninsula since the early 2000s, attributed to both forest expansion on abandoned agricultural land and climate warming, which enhanced photosynthetic activity. Likewise, Mancino et al. (2014) linked NDVI increases in the Basilicata region (southern Italy) to afforestation and forest densification, while Sarvia, De Petris, and Borgogno-Mondino (2021) observed rising NDVI values in areas where land cover remained unchanged, highlighting the role of climatic factors.

The interaction between climate and LULC dynamics is a key factor explaining these patterns. In our study, the documented expansion of forested areas suggests that local land-use changes may have influenced temperature variations over time. Forest ecosystems can affect the local energy balance by retaining heat at night, increasing atmospheric humidity through evapotranspiration, and modifying near-surface microclimates, all of which can contribute to elevated minimum temperatures. Therefore, while regional warming is likely the dominant driver of temperature trends, local processes such as forest expansion may play a secondary but significant role in modulating temperature dynamics. Furthermore, the NDVI increase observed even within stable land-cover areas suggests that vegetation vigour has been affected by changes in management practices. Specifically, the steady NDVI rise in forested areas may reflect reduced or ceased active forest management, such as coppicing, which typically involves periodic cutting to promote regrowth. In actively managed systems, cyclical NDVI fluctuations correspond to canopy removal and recovery (Chirici et al. 2020). The absence of these fluctuations, alongside the persistent upward trend (Figure 9b), supports the hypothesis of progressive abandonment or passive rewilding in forested landscapes, helped by the recorded moderate warming.

Greening of badland landforms has been documented in several Italian regions, and most studies associated this with the land-use and climatic changes. In the Northern Apennines, forest expansion over the past 40 years has led to a marked decrease in Calanchi areas: Coratza and Parenti (2021) reported a 31% decrease in the Secchia catchment (Emilia-Romagna), Bosino, Omran, and Maerker (2019) a 34% decrease in the Oltrepò Pavese area (Lombardy), and La Licata et al. (2023) observed ongoing reforestation and stabilization in the upper Val d'Arda. A similar 31.7% reduction was recorded in the Central Apennines (Tesino and Tronto basins, Marche) between 1988 and 2016, mainly due to natural dynamics (Bufalini et al., 2022). In southern Italy, Piccarreta et al. (2006) and Capolongo et al. (2008) documented badlands reshaping and levelling for durum wheat cultivation in the Agri and Salandrella–Cavone basins, resulting in a 19-39% reduction in degraded terrain. Comparable processes occur worldwide: Ranga et al. (2016) reported a 20% decline in badland extent in the Chambal Valley (India) due to agricultural expansion, and Marzolff et al. (2015) observed similar levelling and gully infilling in Morocco's Souss Valley.

Regarding the study area, several studies reported a decrease in erosion rate over recent decades, along with an increase in forest and natural surfaces (Castaldi and Chiocchini 2012; Torri et al. 2013; Aucelli et al. 2014; Bollati et al. 2016; Amici et al. 2017). Recently, Vergari et al. (2025) conducted an in-depth analysis of landscape changes over the last century: starting in the 1930s, the Upper and Middle Orcia Valley underwent an extensive land reclamation program aimed at transforming a degraded landscape characterized by badland landforms into productive agricultural land. This intervention was part of a broader national effort to improve rural productivity and mitigate soil erosion. Extensive reclamation works, such as land levelling, gully infilling, and reforestation, gradually reduced sediment supply and connectivity between hillslopes and channels, triggering notable fluvial adjustments. In the Formone River, these changes were accompanied by a marked narrowing of the active channel, with average channel width decreasing from about 70 m in 1954 to roughly 35 m in 2019, and by a transition from a braided to a wandering–sinuous single-channel pattern, as indicated by a reduction in braiding index and a concomitant increase in sinuosity, coupled with incision and terrace formation along its course. In conjunction with this, artificial reforestation with conifers such as *Pinus nigra* and *Cupressus arizonica* contributed to stabilizing hillslopes, while natural vegetation recolonization following agricultural abandonment further enhanced this transformation (Vergari et al. 2025).

Concluding, climate warming provides a more favourable background, reducing winter stress and extending the growing season, but it is primarily its interaction with forest expansion, land abandonment, cessation of coppicing, and the intensification of permanent crops that drives widespread greening, thereby limiting the development and spatial persistence of badland areas. This integrated view of climatic and land-use controls on badland stabilization and landscape transformation is summarized in the conceptual framework shown in Figure 11.

4.2. Uncertainties

In this study, multitemporal trends in vegetation dynamics were investigated through the examination of NDVI time series spanning nearly four decades derived from Landsat imagery. While the extensive temporal coverage of the Landsat archive is valuable, achieving a continuous monthly dataset from 1984 to 2023 remains challenging due to data gaps and limitations of high-quality scene availability. To address these issues, NDVI pixels were first filtered using the Pixel Quality Assessment (PQA) band, and the remaining valid observations were mosaicked to obtain the cleanest possible NDVI composites. Even if each

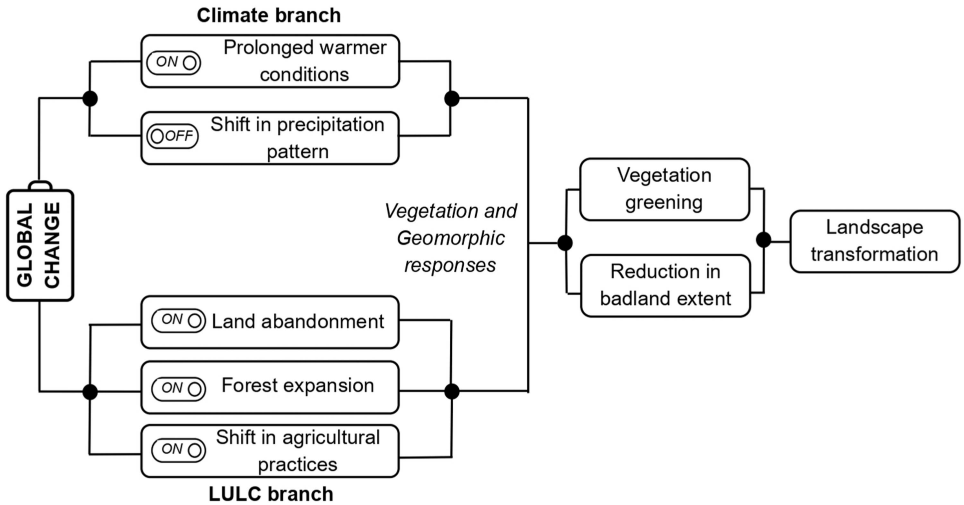

Figure 11. Overview of climatic and land-use controls on badland stabilization and landscape transformation.

composite image retained at least 80% pixel coverage (Figure 3), providing an adequate amount of data for the purposes of this analysis in all seasons, the lowest number of images occurs in the winter months of December, January, and February, as well as in April, which is a particularly rainy month in the study area. This temporal bias is inherent to areas with pronounced seasonality, where clouds and precipitation are strongly seasonal. A similar phenomenon happened to the mountainous sectors of the study area, such as the Monte Amiata region (Figure 1), where the higher frequency of clouds, snow, and topographic shadows reduces the representativeness of high-elevation environments.

Moreover, even the use of the PQA filter and the mosaicking procedure does not fully guarantee the removal of all sources of uncertainty at the pixel level, as residual disturbances such as aerosol, haze, partial cloud cover, and topographic shadows may still affect NDVI values. For this reason, monthly composites were generated by selecting, for each pixel, the highest NDVI value within the month, under the assumption that lower NDVI observations are more likely to be impacted by this residual noise and pixel acquired in a common monthly window do not capture markedly different phenological stages and therefore are comparable in terms of vegetation development (e.g. Didan and Munoz 2021; Robinson et al. 2017). Generally, the use of the non-parametric Mann–Kendall test and Sen's slope helps to mitigate the influence of remaining noise, outlier values, and uneven sampling on trend detection, because these statistics rely on rank information and median slopes rather than on strict distributional assumptions, providing a robust indication of long-term vegetation change.

Likewise, analyzing highly heterogeneous and small-scale landforms such as *Calanchi* and *Biancane*, the spatial resolution of satellite imagery only partially captures subtle or localized changes (Colacicco et al. 2025). NDVI sensitivity varies with vegetation conditions: under low vegetation density, soil background significantly influences NDVI values, whereas at high biomass levels, the index tends to saturate, limiting its responsiveness to further canopy growth (Tian et al. 2025). This is particularly important in badland areas, where sparse vegetation and extensive bare soil can introduce uncertainty when using NDVI as a proxy for exposed land. Variations in NDVI may reflect changes in vegetation cover rather than actual shifts in bare soil area. For example, an increase in NDVI might be interpreted as a reduction in badlands, but it could simply result from seasonal vegetation growth in the same location. To address this limitation, this study used a statistical trend able to detect long-term monotonic trends to avoid misinterpretation of temporary vegetation tendency, accompanied by LULC and climatic information.

The LULC classification used in this study also presents inherent uncertainties. The LULC map of 1980, produced at 1:25.000 scale from black-and-white aerial photographs acquired in 1975–1976, is affected by several intrinsic limitations. The minimum mappable unit was approximately 8 mm^2, and a prevalence criterion was adopted whereby, only the culturally or economically most important class was mapped, implying a likely underestimation of small, fragmented landforms such as badlands. Additional geometric and thematic uncertainties may also derive from the updating process based on the 1979–1980 regional flight (1:33,000), which involved the visual adjustment of polygon boundaries (Regione Toscana – Uso e Copertura del suolo – Scala 1:25.000 – Anno 1978). The most recent maps used (2007, 2010, 2013, 2016, and 2019) were produced at 1:10.000 scale after photointerpretation, with the Minimum Mapping Unit set at 0.5 ha (5000 m^2) for polygon features. The classification follows regional adaptation of the CORINE Land Cover guidelines, designed to reduce interpreter subjectivity through the use of standardized geometric models for each class. According to the official documentation, the thematic accuracy of this dataset, assessed through field surveys on a sample of 2655 elements, is 92.05%, indicating a generally high reliability of class attribution at the mapped scale (Regione Toscana – Uso e copertura del suolo 2007–2019).

4.3. Limitations and future direction

This work aimed to identify clear trends in vegetation development, as well as in precipitation and temperature patterns. The use of multiple satellite-based datasets with different spatial resolutions (i.e. Landsat, MODIS, and GPM) inevitably introduces limitations when comparing results, as coarser products tend to smooth fine-scale spatial heterogeneity. This is particularly critical in heterogeneous landscapes, such as agricultural mosaics and badlands, where small vegetation patches or erosion features may be smaller than a single pixel and thus remain undetected in coarse-resolution data (Moreno de las Heras and Gallart 2017). Higher-resolution satellite imagery, such as Sentinel-2 (10 m) or PlanetScope (~3 m), could improve the detection of small badlands areas and sparse vegetation patches (Andreatta et al. 2022; Sebastiani, Salvati, and Manes 2023). However, these datasets are only available for the last few years, which limits their use for long-term trend analysis spanning multiple decades, as done with Landsat imagery for the long-term purpose of this study. In this study, the extent of badlands was inferred from widely used land-use maps, ensuring consistency and comparability across the large spatial and temporal scales considered in the analysis. Finally, LULC information was only available for five time slices (1980, 2007, 2013, 2016, and 2019), derived from two datasets with different, although still comparable, mapping scales (1980: 1:25,000; 2007–2019: 1:10,000). These datasets do not exactly coincide with the beginning and end of the NDVI analysis period, but they provide a reasonable approximation of the main phases of LULC evolution, also considering that the most drastic LULC changes occurred before the 1980s (Vergari et al. 2025) and that, since 2007, the magnitude of the overall trend appears relatively stable.

This results in a substantial temporal gap, particularly between 1980 and 2007, which may prevent capturing intermediate land cover states and transitions influencing monthly NDVI trends and thus introduces some uncertainty in the interpretation of the role of LULC change in vegetation dynamics. Future research could also benefit from the inclusion of land cover changes derived from additional biophysical indicators, such as the Leaf Area Index (LAI), and from other classification products (Manes et al. 2010). Such integration could help validate the vegetation trends observed through NDVI analysis and provide a more comprehensive understanding of the processes driving land cover evolution. The statistical core of this work relied on the Mann–Kendall test applied in combination with Sen's slope estimator and Pearson's correlation analysis. However, more sophisticated approaches, such as seasonal-trend decomposition of time series or the use of machine learning and deep learning methods, could be adopted in future studies to better capture complex, nonlinear relationships between vegetation dynamics and global change.

5. Conclusion

In this study, Landsat products are used to estimate linear trends in vegetation dynamics over the past four decades (1984–2023) by analyzing the NDVI trends in a rural landscape with badlands located in Central Italy. Trends in climate variables (precipitation and temperature) were investigated using satellite products, including MODIS LST and GPM data, as well as records from regional ground-based meteorological stations for the last two decades (2004–2023). The non-parametric Mann–Kendall test and the associated Sen's slope are applied to quantify these trends. LULC changes are analyzed using several regional land cover maps (1980 and 2007-2019) to evaluate land cover evolution during the study period.

Results reveal generally positive NDVI trends over the full 40-year span, with a pronounced seasonal signal characterized by increasing NDVI values from May to October. The first twenty years (1984–2003) show a limited area affected by significant trends, with a predominance of weak NDVI decline, especially during summer months. In contrast, the most recent two decades (2004–2023) were marked by a substantial increase in the spatial extent of significant NDVI trends, dominated by positive values. This strong increase observed over the last two decades outweighs the earlier negative trends, resulting in an overall positive NDVI trend for the entire 40-year period.

A warming trend, particularly nocturnal temperature rises in summer and winter was detected. Satellite-based precipitation analysis showed no significant change, while ground-based meteorological data indicated only slight localized increases. Agricultural areas decreased overall, with a strong decline in pastures and heterogeneous mosaics, while permanent crops expanded. Forest cover increment across all types, reflecting both natural succession in abandoned lands and targeted afforestation efforts.

Our results indicate that a process of steady revegetation of the rural landscape is underway, also contributing to the decline of active badlands erosional surfaces. These increases in vegetation may therefore be attributed both to the improved climatic conditions, which likely extended the growing season, and to land-use abandonment and changes in land management, which have promoted the expansion of forested areas.

Concluding, the analysis of satellite-based datasets, combined with ground-based meteorological records and long-term LULC maps, has uncovered new insights into the human-induced landscape evolution of a representative Mediterranean rural area characterized by badlands. This study contributes to advancing the understanding of landscape evolution as the combined result of direct and indirect anthropogenic pressures. Direct impacts are primarily associated with land-use changes, while indirect effects are likely linked to ongoing climate change, whose dynamics are still under active investigation. By integrating multi-decadal land-use and NDVI analyses, this research provides new insights into how these drivers interact and shape extremely sensitive environments such as badlands.

The results highlight that even over relatively short temporal scales, the landscapes can undergo substantial transformations in response to complex and combined human pressures. These findings not only improve our understanding of long-term landscape trajectories but also offer valuable knowledge to support territorial planning and watershed management. Furthermore, they may inform strategies and policies aimed at mitigating hydro-meteorological hazards by emphasizing the importance of anticipating how ecosystems respond to changing climatic and land-use conditions.

Finally, while the growth-oriented policies of the past century transformed arid clay soils into productive farmland (often at the expense of geomorphological heritage), contributing to the creation of a typical rural landscape, current trends of land abandonment now threaten to erase those efforts. Paradoxically, this passive form of landscape preservation is also undermining the ecological value of these environments: the encroachment of ruderal vegetation onto formerly bare badland surfaces is leading to the loss of pioneer plant communities and endemic species, resulting in a measurable decline in biodiversity even within protected areas (Torri et al. 2013). The Orcia Valley exemplifies this paradox of rural landscape transformation: a territory once stabilized and cultivated through intentional human intervention is now increasingly vulnerable to degradation driven by neglect and spontaneous rewilding. What is often perceived today as a "natural" landscape is, in fact, a cultural construct, one that risks disappearing without active care, formal recognition, and adaptive management strategies.

Author contributions

CRediT: **Annalisa Sannino:** Conceptualization, Data curation, Formal analysis, Methodology, Software, Writing – original draft; **Ebrahim Ghaderpour:** Conceptualization, Methodology, Supervision, Validation, Writing – review & editing; **Giulia Iacobucci:** Conceptualization, Writing – review & editing; **Maurizio Del Monte:** Conceptualization, Writing – review & editing; **Francesca Vergari:** Conceptualization, Funding acquisition, Methodology, Supervision, Validation, Writing – review & editing.

Disclosure statement

No potential conflict of interest was reported by the author(s).

Funding

This study is supported by National Recovery and Resilience Plan (NRRP) Mission 4, Component 2, Investment 1.1 "Fund for the National Research and Projects Programme of Significant National Interest (PRIN2022)" funded by the European Union—Next Generation EU CUP B53D23007030006 – ERC PE10 – Code 2022C7K7RR (PRIN2022 Project "BAD2BED – BADland morphodynamics assessment and hillslopechannel BED coupling in the context of global change," PI Francesca Vergari). The first author has a grant funded by National Recovery and Resilience Plan (NRRP) Mission 4 Component 2 Investment 4.1, CUP B53C23002180006 funded by the European Union, Next Generation EU.

ORCID

Annalisa Sannino 0009-0005-6600-6629
Ebrahim Ghaderpour 0000-0002-5165-1773
Giulia Iacobucci 0000-0002-1419-1536
Maurizio Del Monte 0000-0002-9564-3548
Francesca Vergari 0000-0002-5552-0797

Data availability statement

The data that support the findings of this study are openly available in Zenodo at http://doi.org/10.5281/zenodo.17661626 under the CC-BY license (Sannino et al. 2026).

References

Acocella, V., and F. Rossetti. 2002. "The Role of Extensional Tectonics at Different Crustal Levels on Granite Ascent and Emplacement: An Example from Tuscany (Italy)." *Tectonophysics* 354 (1-2): 71–83. https://doi.org/10.1016/S0040-1951(02)00290-1.

Agnoletti, M. 2007." The degradation of traditional landscape in a mountain area of Tuscany during the 19th and 20th centuries: Implications for biodiversity and sustainable management." *Forest Ecology and Management* 249(1-2): 5–17. 5-17. https://doi.org/10.1016/j.foreco.2007.05.032.

Agnoletti, M, ed. 2012. Italian Historical Rural Landscapes. In *Cultural values for the environment and rural development*. Dordrecht: Springer Verlag.

Agnoletti, M., F. Piras, M. Venturi, and A. Santoro. 2022. "Cultural values and forest dynamics: The Italian forests in the last 150 years." *Forest Ecology and Management* 503: 119655. 119655. https://doi.org/10.1016/j.foreco.2021.119655.

Amici, V., S. Maccherini, E. Santi, D. Torri, F. Vergari, and M. Del Monte. 2017. "Long-Term Patterns of Change in a Vanishing Cultural Landscape: A GIS-based Assessment." *Ecological Informatics* 37: 38–51. https://doi.org/10.1016/j.ecoinf.2016.11.008.

Andreatta, D., D. Gianelle, M. Scotton, and M. Dalponte. 2022. "Estimating Grassland Vegetation Cover with Remote Sensing: A Comparison between Landsat-8, Sentinel-2 and PlanetScope Imagery." *Ecological Indicators* 141: 109102. https://doi.org/10.1016/j.ecolind.2022.109102.

Asare, Y. M., E. K. Forkuo, G. Forkuor, and M. Thiel. 2020. "Evaluation of Gap-Filling Methods for Landsat 7 ETM+ SLC-off Image for LULC Classification in a Heterogeneous Landscape of West Africa." *International Journal of Remote Sensing* 41 (7): 2544–2564. https://doi.org/10.1080/01431161.2019.1693076.

Aucelli, P.P. C., M. Conforti, M. Della Seta, M. Del Monte, L. D'uva, C.M. Rosskopf, and F. Vergari. 2014. "Multi-temporal Digital Photogrammetric Analysis for Quantitative Assessment of Soil Erosion Rates in the Landola Catchment of the Upper Orcia Valley (Tuscany, Italy)." *Land Degradation & Development* 27(4): 1075–1092. 1075-1092. https://doi.org/10.1002/ldr.2324.

Bajocco, S., A. De Angelis, L. Perini, A. Ferrara, and L. Salvati. 2012. "The Impact of Land Use/Land Cover Changes on Land Degradation Dynamics: A Mediterranean Case Study." *Environmental Management* 49: 980–989. https://doi.org/10.1007/s00267-012-9831-8.

Bajocco, S., C. Ferrara, A. Alivernini, M. Bascietto, and C. Ricotta. 2019. "Remotely-Sensed Phenology of Italian Forests: Going Beyond the Species." *International Journal of Applied Earth Observation and Geoinformation* 74: 314–321. https://doi.org/10.1016/j.jag.2018.10.003.

Bellini, E., R. Martin, G. Argenti, N. Staglianò, C. Dibari, M. Moriondo, and G. Bellocchi. 2023. "Opportunities for Adaptation to Climate Change of Extensively Grazed Pastures in the Central Apennines (Italy)." *Land* 12 (2): 351. https://doi.org/10.3390/land12020351.

Blondel, J. 2006. "The 'Design' of Mediterranean Landscapes: A Millennial Story of Humans and Ecological Systems during the Historic Period." *Human Ecology* 34 (2006): 713–729. https://doi.org/10.1007/s10745-006-9030-4.

Boccolari, M., and S. Malmusi. 2013. "Changes in Temperature and Precipitation Extremes Observed in Modena, Italy." *Atmospheric Research* 122: 16–31. https://doi.org/10.1016/j.atmosres.2012.10.022.

Bollati, I., F. Vergari, M. Del Monte, and M. Pelfini. 2016. "Multitemporal dendrogeomorphological analysis of slope instability in Upper Orcia Valley (Southern Tuscany, Italy". *Geogr. Fis. Din. Quat.* 39 (2), 105–120. https://doi.org/10.4461/GFDQ2016.39.10.

Bosino, A., A. Omran, and M. Maerker. 2019. "Identification, Characterisation and Analysis of the Oltrepo Pavese Calanchi in the Northern Apennines (Italy)." *Geomorphology* 340: 53–66. https://doi.org/10.1016/j.geomorph.2019.05.003.

Brandolini, F., C. Compostella, M. Pelfini, and S. Turner. 2023. "The Evolution of Historic Agroforestry Landscape in the Northern Apennines (Italy) and Its Consequences for Slope Geomorphic Processes." *Land* 12 (5): 1054. https://doi.org/10.3390/land12051054.

Brandolini, P., A. Cevasco, D. Capolongo, G. Pepe, F. Lovergine, and M. D. Monte. 2018. "Response of Terraced Slopes to a Very Intense Rainfall Event and Relationships with Land Abandonment: A Case Study from Cinque Terre (Italy)." *Land Degradation & Development* 29 (3): 630–642. https://doi.org/10.1002/ldr.2672.

Brandolini, P., C. Cappadonia, G. M. Luberti, C. Donadio, L. Stamatopoulos, C. D. Maggio, F. Faccini, et al. 2020. "Geomorphology of the Anthropocene in Mediterranean Urban Areas." *Progress in Physical Geography: Earth and Environment* 44: 461–494. https://doi.org/10.1177/0309133319881108.

Bryan, R. B., and A. Yair. 1982. (Eds.), Badland Geomorphology and Piping. Norwich, United Kingdom: Geo Books.

Bufalini, M., A. Omran, and A. Bosino. 2022. "Assessment of Badlands Erosion Dynamics in the Adriatic Side of Central Italy." *Geosciences* 12(5): 208. 208. https://doi.org/10.3390/geosciences12050208.

Cannone, N., S. Sgorbati, and M. Guglielmin. 2007. "Unexpected Impacts of Climate Change on Alpine Vegetation." *Frontiers in Ecology and the Environment* 5 (7): 360–364. https://doi.org/10.1890/1540-9295(2007)5[360:UIOCCO]2.0.CO;2.

Capolongo, D., L. Pennetta, M. Piccarreta, G. Fallacara, and F. Boenzi. 2008. "Spatial and Temporal Variations in Soil Erosion and Deposition Due to Land-Levelling in a Semi-Arid Area of Basilicata (Southern Italy)." *Earth Surface Processes and Landforms* 33 (3): 364–379. https://doi.org/10.1002/esp.1560.

Castaldi, F., and U. Chiocchini. 2012. "Effects of Land Use Changes on Badland Erosion in Clayey Drainage Basins, Radicofani, Central Italy." *Geomorphology* 169-170: 98–108. https://doi.org/10.1016/j.geomorph.2012.04.016.

Cavalli, A., S. Francini, G. Cecili, C. Cocozza, L. Congedo, V. Falanga, G. L. Spadoni, et al. 2022. "Afforestation Monitoring through Automatic Analysis of 36-Years Landsat Best Available Composites." *iForest - Biogeosciences and Forestry* 15 (4): 220–228. https://doi.org/10.3832/ifor4043-015.

Chelli, S., C. Wellstein, G. Campetella, R. Canullo, R. Tonin, S. Zerbe, and R. Gerdol. 2017. "Climate Change Response of Vegetation Across Climatic Zones in Italy." *Climate Research* 71(3): 249–262. https://doi.org/10.3354/cr01443.

Chen, X., Z. Su, Y. Ma, J. Cleverly, and M. Liddell. 2017. "An Accurate Estimate of Monthly Mean Land Surface Temperatures from MODIS Clear-Sky Retrievals." *J. Hydrometeor.* 18: 2827–2847. https://doi.org/10.1175/JHM-D-17-0009.1.

Chirici, G., F. Giannetti, E. Mazza, S. Francini, D. Travaglini, R. Pegna, and J. C. White. 2020. "Monitoring Clearcutting and Subsequent Rapid Recovery in Mediterranean Coppice Forests with Landsat Time Series." *Annals of Forest Science* 77: 40. https://doi.org/10.1007/s13595-020-00936-2.

Ciccacci, S., M. Galiano, M. A. Roma, and M. C. Salvatore. 2008. "Morphological Analysis and Erosion Rate Evaluation in Badlands of Radicofani Area (Southern Tuscany — Italy)." *Catena* 74 (2): 87–97. https://doi.org/10.1016/j.catena.2008.03.012.

Ciotoli, G., M. Della Seta, M. Del Monte, P. Fredi, S. Lombardi, E. Lupia Palmieri, and F. Pugliese. 2003. "Morphological and Geochemical Evidence of Neotectonics in the Volcanic Area of Monti Vulsini (Latium, Italy)." *Quaternary International* 101-102: 103–113. https://doi.org/10.1016/S1040-6182(02)00093-9.

Colacicco, R., M. La Salandra, I. Lapietra, A. Refice, and D. Capolongo. 2025. "Remote Sensing Techniques to Assess Badlands Dynamics: Insights from a Systematic Review." *GIScience & Remote Sensing* 62(1): 1-34. https://doi.org/10.1080/15481603.2025.2516347.

Coratza, P., and C. Parenti. 2021. "Controlling Factors of Badland Morphological Changes in the Emilia Apennines (Northern Italy)." *Water* 13(4): 539. https://doi.org/10.3390/w13040539.

Crawford, C. J., D. P. Roy, S. Arab, C. Barnes, E. Vermote, G. Hulley, A. Gerace, et al. 2023. "The 50-Year Landsat Collection 2 Archive." *Science of Remote Sensing* 8: 100103. https://doi.org/10.1016/j.srs.2023.100103.

De Angelis, A., S. Bajocco, and C. Ricotta. 2012. "Modelling the Phenological Niche of Large Fires with Remotely Sensed NDVI Profiles." *Ecological Modelling* 228: 106–111. https://doi.org/10.1016/j.ecolmodel.2012.01.003.

Del Monte, M. 2017. The Typical Badlands Landscapes between the Tyrrhenian Sea and the Tiber River. In *Landscapes and Landforms of Italy*. *World Geomorphological Landscapes*. M. Soldati and M. Marchetti, eds. 281–291, Cham: Springer. https://doi.org/10.1007/978-3-319-26194-2_24.

Didan, K., and Munoz, A. B. 2021. MODIS Collection 6.1 Vegetation Index Product User Guide (MOD13 Series), LP DAAC/USGS.

Feller, U., and I. I. Vaseva. 2014. "Extreme Climatic Events: Impacts of Drought and High Temperature on Physiological Processes in Agronomically Important Plants." *Frontiers in Environmental Science* 2: 108115. https://doi.org/10.3389/fenvs.2014.00039.

Fibbi, L., M. Moriondo, M. Chiesi, M. Bindi, and F. Maselli. 2019. "Impacts of Climate Change on the Gross Primary Production of Italian Forests." *Annals of Forest Science* 76: 59. https://doi.org/10.1007/s13595-019-0843-x.

Fresta. 2011. “La Val d'Orcia: Ovvero L'Invenzione Di Un Paesaggio Tipico Toscano.” *Lares* 77 (2): 205–218. http://www.jstor.org/stable/26231341.
Gabriele, M., R. Brumana, M. Previtali, and A. Cazzani. 2023. “A Combined GIS and Remote Sensing Approach for Monitoring Climate Change-Related Land Degradation to Support Landscape Preservation and Planning Tools: The Basilicata Case Study.” *Appl Geomat* 15: 497–532. https://doi.org/10.1007/s12518-022-00437-z.
Gallardo, M., J. Fernández-Portela, D. Cocero, and L. Vilar. 2023. “Land Use and Land Cover Changes in Depopulated Areas of Mediterranean Europe: A Case Study in Two Inland Provinces of Spain.” *Land* 12 (11): 1967. https://doi.org/10.3390/land12111967.
Gallart, F., M. Marignani, N. Pérez-Gallego, E. Santi, and S. Maccherini. 2013. “Thirty Years of Studies on Badlands, from Physical to Vegetational Approaches. a Succinct Review.” *CATENA* 106: 4–11. https://doi.org/10.1016/j.catena.2012.02.008.
Ghaderpour, E., and T. Vujadinovic. 2020. “Change Detection Within Remotely Sensed Satellite Image Time Series Via Spectral Analysis.” *Remote Sensing* 12 (23): 4001. https://doi.org/10.3390/rs12234001.
Ghaderpour, E., P. Mazzanti, G. S. Mugnozza, and F. Bozzano. 2023. “Coherency and Phase Delay Analyses between Land Cover and Climate Across Italy Via the Least-Squares Wavelet Software.” *International Journal of Applied Earth Observation and Geoinformation* 118: 103241. https://doi.org/10.1016/j.jag.2023.103241.
Ghaderpour, E., P. Mazzanti, F. Bozzano, and G. Scarascia Mugnozza. 2024. “Trend Analysis of MODIS Land Surface Temperature and Land Cover in Central Italy.” *Land* 13 (6): 796. https://doi.org/10.3390/land13060796.
Ghaderpour, E., F. Bozzano, G. Scarascia Mugnozza, and P. Mazzanti. 2025. “Analyses of MODIS Land Cover/Use and Wildfires in Italian Regions Since 2001.” *Land 2025* 14 (7): 1443. https://doi.org/10.3390/land14071443.
Giaccone, E., F. Vergari, M. Del Monte, and S. Fratianni. 2015. L'impact Du Climat Sur Les Dynamiques Morphologiques En Toscane (Italie Centrale). In *Proceedings of the “XXVIIIe Colloque de l'Association Internationale de Climatologie”*. Liège.
Gilman, J., and J. Wu. 2023. “The Interactions Among Landscape Pattern, Climate Change, and Ecosystem Services: Progress and Prospects.” *Reg Environ Change* 23: 67. https://doi.org/10.1007/s10113-023-02060-z.
Harvey, A., 2004. Badland. In: Goudie, A.S. (Ed.), Encyclopedia of Geomorphology. Routledge, pp. 45–48.
Huang, S., L. Tang, J. P. Hupy, Y. Wang, and G. Shao. 2021. “A Commentary Review on the Use of Normalized Difference Vegetation Index (NDVI) in the Era of Popular Remote Sensing.” *Journal of Forestry Research* 32: 1–6. https://doi.org/10.1007/s11676-020-01155-1.
Hussain, M., and I. Mahmud. 2019. “pyMannKendall: A Python Package for Non Parametric Mann Kendall Family of Trend Tests.” *Journal of Open Source Software* 4(39): 1556. https://doi.org/10.21105/joss.01556.
Karpouzos, D. K., S. Kavalieratou, and C. Babajimopoulos. 2010. “Trend Analysis of Precipitation Data in Pieria Region (Greece).” *Europe Water* 30: 31–40.
Kašanin-Grubin, M., F. Vergari, F. Troiani, and M. Della Seta. 2018. “The Role of Lithology: Parent Material Controls on Badland Development. In: E. Nadal-Romero, J.F. MartÍNez-Murillo, N. Khun, *Badlands Dynamics in the Context of Global Change*. 61–109. Amsterdam: Elsevier. https://doi.org/10.1016/B978-0-12-813054-4.00003-4.
Kendall, M. G. 1938. “A New Measure of Rank Correlation.” *Biometrika* 30 (1-2): 81–93. https://doi.org/10.1093/biomet/30.1-2.81.
Kizos, T., A. Dalaka, and T. Petanidou. 2010. “Farmers' Attitudes and Landscape Change: Evidence from the Abandonment of Terraced Cultivations on Lesvos, Greece.” *Agriculture and Human Values* 27: 199–212. https://doi.org/10.1007/s10460-009-9206-9.
Kumar, R., K. Jalem, S. K. Swain, S. Kanga, S. K. Singh, G. Meraj, P. Kumar, and D. Mandal. 2025. “Geospatial Analysis of Climate-Induced Land Cover Changes and Vegetation Trends in Western Jharkhand, India.” *Environmental Monitoring and Assessment* 197: 1019. https://doi.org/10.1007/s10661-025-14452-1.
La Licata, M., A. Bosino, M. Bettoni, and M. Maerker. 2023. “Assessing landscape features and geomorphic processes influencing sediment dynamics in a geomorphologically highly active Mediterranean agroecosystem: The upper Val d'Arda case study (Northern Apennines, Italy).” *Geomorphology* 433: 108724. 108724. https://doi.org/10.1016/j.geomorph.2023.108724.
Liotta, D. 1996. “Analisi Del Settore Centromeridionale Del Bacino Pliocenico Di Radicofani (Toscana Meridionale).” *Bollettino della Societa Geologica Italiana* 115: 115–143. https://hdl.handle.net/11586/41614.
Llena, M., D. Vericat, M. Cavalli, S. Crema, and M. W. Smith. 2019. “The Effects of Land Use and Topographic Changes on Sediment Connectivity in Mountain Catchments.” *Science of The Total Environment* 660: 899–912. https://doi.org/10.1016/j.scitotenv.2018.12.479.
Mancino, G., A. Nole, F. Ripullone, and A.M.S. Ferrara. 2014. “Landsat TM Imagery and NDVI Differencing for Vegetation Change Detection: Assessing Natural Expansion of Forests in Basilicata, Southern Italy.” *iForest* 7: 75–84. http://www.sisef.it/iforest/contents/?id=ifor0909-007.
Manes, F., C. Ricotta, E. Salvatori, S. Bajocco, and C. Blasi. 2010. “A Multiscale Analysis of Canopy Structure in *Fagus Sylvatica* L. and *Quercus Cerris* L. Old-Growth Forests in the Cilento and Vallo Di Diano National Park.” *Plant Biosystems - An International Journal Dealing with All Aspects of Plant Biology* 144 (1): 202–210. https://doi.org/10.1080/11263500903560801.
Mann, H. B. 1945. “Nonparametric Tests against Trend.” *Econometrica* 13 (3): 245–259. https://doi.org/10.2307/1907187.

Martinez-Harms, M. J., B. A. Bryan, E. Figueroa, P. Pliscoff, R. K. Runting, and K. A. Wilson. 2017. "Scenarios for Land Use and Ecosystem Services under Global Change." *Ecosystem Services* 25: 56–68. https://doi.org/10.1016/j.ecoser.2017.03.021.

Marzolff, I., P. Pani, S. N. Mohapatra, Ghafrani, and A. Ait Hssaine. 2015. Sustainability of Land Reclamation Measures in Erosional Badlands: A Comparative Perspective on Semi-Arid Landscapes of South Morocco and Central India In *Geophysical Research Abstracts*. Vol. 17. EGU2015-9825, 2015.

Maselli, F. 2004. "Monitoring Forest Conditions in a Protected Mediterranean Coastal Area By the Analysis of Multiyear NDVI Data." *Remote Sensing of Environment* 89 (4): 423–433. https://doi.org/10.1016/j.rse.2003.10.020.

Moreno de las Heras, M., and F. Gallart. 2017. "The Application of Land Morphology and Lithology Information Optimizes Remote Sensing Badland Mapping Using Landsat 8 and Sentinel 2 Imagery in a Heterogeneous Regional Setting, the Upper Llobregat Basin (Catalan Pyrenees)." *In EGU General Assembly Conference Abstracts* 19: 13950–13950.

Nadal-Romero, E., S. M. Vicente-Serrano, and I. Jiménez. 2012. "Assessment of Badland Dynamics Using Multi-Temporal Landsat Imagery: An Example from the Spanish Pre-Pyrenees." *Catena* 96: 1–11. https://doi.org/10.1016/j.catena.2012.03.010.

Nadal-Romero, E., E. Rodríguez-Caballero, S. Chamizo, C. Juez, Y. Cantón, and J. M. García-Ruiz. 2021. "Mediterranean Badlands: Their Driving Processes and Climate Change Futures." *Earth Surface Processes and Landforms* 47 (1): 17–31. https://doi.org/10.1002/esp.5088.

Neugirg, F., M. Stark, A. Kaiser, M. Vlacilova, M. Della Seta, F. Vergari, J. Schmidt, M. Becht, and F. Haas. 2016. "Erosion Processes in Calanchi in the Upper Orcia Valley, Southern Tuscany, Italy Based on Multitemporal High-Resolution Terrestrial LiDAR and UAV Surveys." *Geomorphology* 269: 8–22. https://doi.org/10.1016/j.geomorph.2016.06.027.

Pettorelli, N., J. O. Vik, A. Mysterud, J. M. Gaillard, C. J. Tucker, and N. C. Stenseth. 2005. "Using the Satellite-Derived NDVI to Assess Ecological Responses to Environmental Change." *Trends in Ecology & Evolution* 20: 503–510. https://doi.org/10.1016/j.tree.2005.05.011.

Piccarreta, M., D. Capolongo, F. Boenzi, and M. Bentivenga. 2006. "Implications of decadal changes in precipitation and land use policy to soil erosion in Basilicata, Italy." *CATENA* 65(2): 138–151. 138-151. https://doi.org/10.1016/j.catena.2005.11.005.

Ranga, V., J. Poesen, A. Van Rompaey, S. N. Mohapatra, and P. Pani. 2016. "Detection and Analysis of Badlands Dynamics in the Chambal River Valley (India), during the Last 40 (1971–2010) Years." *Environmental Earth Sciences* 75: 183. https://doi.org/10.1007/s12665-015-5017-z.

Ratner, B. 2009. "The Correlation Coefficient: Its Values Range between +1/−1, or Do They?" *Journal of Targeting, Measurement and Analysis for Marketing* 17 (2): 139–142. https://doi.org/10.1057/jt.2009.5.

Regione Toscana – "Uso e Copertura del suolo - Scala 1:25.000 - Anno 1978". Last accessed 28/04/2025. https://www502.regione.toscana.it/geoscopio/download/tematici/ucs_rt_1978_25k/index.html?catIdx=0%2F6&layIdx=4&tolobbox=424789.15359401:903921.96640599:4675060:4929665.5&tolosrid=EPSG%3A25832&tolozoom=1601142.3949417635&tololayerserver=https%3A%2F%2Fwww502.regione.toscana.it%3A443%2Fwmsraster%2Fcom.rt.wms.RTmap%2Fwms%3Fmap%3Dwmssfondo%26version%3D1.1.1%26map_mnt%3Dcartoteca&tololayername=a.

Regione Toscana – "Uso e copertura del suolo 2007-2019". Last accessed 28/04/2025. https://www502.regione.toscana.it/geoscopio/download/tematici/ucs_rt/index.html?catIdx=0%2F6&layIdx=0&tolobbox=424789.15359401:903921.96640599:4675060:4929665.5&tolosrid=EPSG%3A25832&tolozoom=1601142.3949417635&tololayerserver=https%3A%2F%2Fwww502.regione.toscana.it%3A443%2Fwmsraster%2Fcom.rt.wms.RTmap%2Fwms%3Fmap%3Dwmssfondo%26version%3D1.1.1%26map_mnt%3Dcartoteca&tololayername=a.

Regione Toscana - Servizio Idrologico Regionale – portale SIR: Last accessed on 28/04/2025. https://www.sir.toscana.it/.

Ricotta, C., P. Corona, and M. Marchetti. 1999. "Informational Analysis of Forest Landscape Spatial Heterogeneity." *Journal of Sustainable Forestry* 9 (1–2): 97–106. https://doi.org/10.1300/J091v09n01_08.

Robinson, N. P., B. W. Allred, M. O. Jones, A. Moreno, J. S. Kimball, D. E. Naugle, T. A. Erickson, and A. D. Richardson. 2017. "A Dynamic Landsat Derived Normalized Difference Vegetation Index (NDVI) Product for the Conterminous United States." *Remote Sensing* 9: 863. https://doi.org/10.3390/rs9080863.

Sannino, A., E. Ghaderpour, G. Iacobucci, M. Del Monte, and F. Vergari. 2026. "Insights into Global Change Effects on a Mediterranean Rural Landscape with Badlands: A Remote Sensing Approach on Climate and Land Cover Changes [Data Set]." *GIScience & Remote Sensing. Zenodo*, https://doi.org/10.5281/zenodo.17661626.

Sarvia, F., S. De Petris, and E. Borgogno-Mondino. 2021. "Climate Change Effects on Vegetation Phenology By MOD13Q1 Data: The Piemonte Region Case Study in the Period 2001–2019." *Agronomy* 11: 555. https://doi.org/10.3390/agronomy11030555.

Sebastiani, A., R. Salvati, and F. Manes. 2023. "Comparing Leaf Area Index Estimates in a Mediterranean Forest Using Field Measurements, Landsat 8, and Sentinel-2 Data." *Ecological Processes* 12: 28. https://doi.org/10.1186/s13717-023-00441-0.

Sen, P. K. 1968. "Estimates of the Regression Coefficient Based on Kendall'S Tau." *Journal of the American Statistical Association* 63 (324): 1379–1389. https://doi.org/10.1080/01621459.1968.10480934.

Shelestov, A., M. Lavreniuk, N. Kussul, A. Novikov, and S. Skakun. 2017. "Exploring Google Earth Engine Platform for Big Data Processing: Classification of Multi-Temporal Satellite Imagery for Crop Mapping." *Frontiers in Earth Science* 5: 232994. https://doi.org/10.3389/feart.2017.00017.

Šímová, P., and K. Gdulová. 2012. "Landscape Indices Behavior: A Review of Scale Effects." *Applied Geography* 34: 385–394. https://doi.org/10.1016/j.apgeog.2012.01.003.

Stark, M., F. Neugirg, A. Kaiser, M. Della Seta, J. Schmidt, M. Becht, and F. Haas. 2020. "Calanchi Badlands Reconstructions and Long-Term Change Detection Analysis from Historical Aerial and UAS Image Processing." *Journal of Geomorphology* 1(1): 2–24. https://doi.org/10.1127/jgeomorpholRJ\/2020/0658.

Tian, Z., J. Fan, T. Yu, N. De Leon, S. M. Kaeppler, and Z. Zhang. 2025. "Mitigating NDVI Saturation in Imagery of Dense and Healthy Vegetation." *ISPRS Journal of Photogrammetry and Remote Sensing* 227: 234–250. https://doi.org/10.1016/j.isprsjprs.2025.06.013.

Torri, D., E. Santi, M. Marignani, M. Rossi, L. Borselli, and S. Maccherini. 2013. "The Recurring Cycles of Biancana Badlands: Erosion, Vegetation, and Human Impact." *Updating Badlands Research Catena* 106: 22–30. https://doi.org/10.1016/j.catena.2012.07.001.

Tuel, A., and E. A. B. Eltahir. 2020. "Why Is the Mediterranean a Climate Change Hot Spot?" *Journal of Climate* 33: 5829–5843. https://doi.org/10.1175/JCLI-D-19-0910.1.

U.S. Geological Survey. 2019. Landsat 7 SLC-off gap-filled products: Phase two methodology. U.S. Geological Survey. Last accessed on 10/03/2026. https://www.usgs.gov/media/files/landsat-7-slc-gap-filled-products-phase-two-methodology.

U.S. Geological Survey. 2023. Landsat 4-7 Collection 2 Level-2 Science Product Guide (Version 4.0, LSDS-1618). U.S. Department of the Interior. Last accessed on 04/07/2025. https://d9-wret.s3.us-west-2.amazonaws.com/assets/palladium/production/s3fs-public/media/files/LSDS-1618_Landsat-4-7_C2-L2-ScienceProductGuide-v4.pdf.

U.S. Geological Survey. 2023. Landsat 8–9 Collection 2 Level-2 Science Product Guide (Versione 6.0, LSDS-1619). U.S. Department of the Interior. https://d9-wret.s3.us-west-2.amazonaws.com/assets/palladium/production/s3fs-public/media/files/LSDS-1619_Landsat8-9-Collection2-Level2-Science-Product-Guide-v6.pdf. Last accessed on 04/07/2025.

U.S. Geological Survey. 2024. Landsat normalized difference vegetation index. https://www.usgs.gov/landsat-missions/landsat-normalized-difference-vegetation-index.

UNESCO. Last accessed on 04/07/2025. https://whc.unesco.org/en/list/1026/.

Velastegui-Montoya, A., N. Montalván-Burbano, P. Carrión-Mero, H. Rivera-Torres, L. Sadeck, and M. Adami. 2023. "Google Earth Engine: A Global Analysis and Future Trends." *Remote Sensing* 15(14): 3675. https://doi.org/10.3390/rs15143675.

Vergari, F., M. Della Seta, M. Del Monte, and M. Barbieri. 2013. "Badlands Denudation "hot spots": The Role of Parent Material Properties on Geomorphic Processes in 20-Years Monitored Sites of Southern Tuscany (Italy)." *Catena* 106: 31–41. https://doi.org/10.1016/j.catena.2012.02.007.

Vergari, F., F. Troiani, M. Cavalli, H. Faulkner, and M. Del Monte. 2025. "Shifts in Hillslope-Channel Connectivity after Land Reclamation in a Mediterranean Semi-Humid Badland Landscape." *Catena* 254: 108921. https://doi.org/10.1016/j.catena.2025.108921.

Vergari, F., H. Faulkner, M. Del Monte, M. Della Seta, S. Ciccacci, and P. Fredi. 2019. "The Use of the slope–area Function to Analyse Process Domains in Complex Badland Landscapes." *Earth Surface Processes and Landforms* 44 (1): 273–286. https://doi.org/10.1002/esp.4496.

Vicente-Serrano, S. M., C. Gouveia, J. J. Camarero, S. Beguería, R. Trigo, J.I. López-Moreno, C. Azorín-Molina, E. Pasho, J. Lorenzo-Lacruz, J. Revuelto, E. Morán-Tejeda, and A. Sanchez-Lorenzo. 2012. "Response of vegetation to drought time-scales across global land biomes." Proceedings of the National Academy of Sciences 110(1): 52–57. 52-57. https://doi.org/10.1073/pnas.1207068110.

Wu, H., and Z. L. Li. 2009. "Scale Issues in Remote Sensing: A Review on Analysis, Processing and Modeling." *Sensors (Basel, Switzerland)* 9 (3): 1768–1793. https://doi.org/10.3390/s90301768.

Xue, J., and B. Su. 2017. "Significant Remote Sensing Vegetation Indices: A Review of Developments and Applications." *Journal of Sensors* 2017: 1–17. https://doi.org/10.1155/2017/1353691.

Yin, G., G. Mariethoz, Y. Sun, and M. F. McCabe. 2017. "A Comparison of Gap-Filling Approaches for Landsat-7 Satellite Data." *International Journal of Remote Sensing* 38 (23): 6653–6679. https://doi.org/10.1080/01431161.2017.1363432.

Zgłobicki, W., J. Poesen, M. Daniels, M. Del Monte, A. J. Guerra, V. Joshi, and A. Sol´eBenet. 2018. Geotouristic Value of Badlands. In *Badlands Dynamics in a Context of Global Change* 277–313.Elsevier. Amsterdam, Netherlands. https://doi.org/10.1016/B978-0-12-813054-4.00009-5.